Geochemistry Geophysics Geosystems G3
AN ELECTRONIC JOURNAL OF THE EARTH SCIENCES
Published by AGU and the Geochemical Society

Article
Volume 7, Number 12
12 December 2006
Q12O04, doi:10.1029/2006GC001316
ISSN: 1525-2027

Magmatic processes in developing oceanic crust revealed in a cumulate xenolith collected at the East Pacific Rise, 9°50′N

W. Ian Ridley
U.S. Geological Survey, Denver Federal Center, Box 25046, Denver, Colorado 80225, USA (iridley@usgs.gov)

Michael R. Perfit and Matthew C. Smith
Department of Geological Sciences, University of Florida, Gainesville, Florida 32611, USA

Daniel J. Fornari
Department of Geology and Geophysics, Woods Hole Oceanographic Institution, Woods Hole, Massachusetts 02543, USA

[1] The petrology and geochemistry of a xenolith, a fragment of a melt-bearing cumulate, within a recently erupted mid-ocean ridge (MOR) lava flow provide information on petrogenetic processes occurring within the newly forming oceanic crust beneath the northern East Pacific Rise (NEPR). The xenolith reveals important petrologic information about MOR magmatic systems concerning (1) melt distribution in a crystal-dominated mush; (2) melt-crystal reactions within the mush; (3) the chemistry of melts that have contributed to the cumulate lithology; and (4) the chemistry of axial melts that enter the axial magma system. The xenolith was enclosed within a moderately primitive, normal mid-ocean ridge basalt (NMORB) erupted in 1991 within the neovolcanic zone of the NEPR, at approximately 9°50′N. The sample is a matrix-dominated, cumulate olivine anorthosite, composed of anorthite (An_{94-90}) and bytownite (An_{89-70}), intergranular olivine ($Fo_{86\pm0.3}$), minor sulfide and spinel, and intergranular glass. Marginal corrosion of plagioclase, and possibly olivine, and internal remelting of plagioclase indicate syntexis. It is surmised that the pore volume was eviscerated several times with moderately primitive basaltic melts and reduced by intergranular crystallization of forsteritic olivine. The presence of anorthite as a cumulate phase in the xenolith and the observation of anorthite xenocrysts in NMORB lavas, and as a cumulate phase in ophiolite gabbros, indicate that Ca-rich melts that are not a part of the NMORB lineage play an important role in the construction of the oceanic crust.

Components: 13,113 words, 16 figures.

Keywords: ridge; xenolith; mid-ocean ridge basalt; syntexis; cumulate; crystal mush.

Index Terms: 1032 Geochemistry: Mid-oceanic ridge processes (3614, 8416); 1036 Geochemistry: Magma chamber processes (3618); 1021 Geochemistry: Composition of the oceanic crust.

Received 27 March 2006; **Revised** 6 August 2006; **Accepted** 11 September 2006; **Published** 12 December 2006.

Ridley, W. I., M. R. Perfit, M. C. Smith, and D. J. Fornari (2006), Magmatic processes in developing oceanic crust revealed in a cumulate xenolith collected at the East Pacific Rise, 9°50′N, *Geochem. Geophys. Geosyst.*, *7*, Q12O04, doi:10.1029/2006GC001316.

Theme: Formation and Evolution of Oceanic Crust Formed at Fast Spreading Rates
Guest Editors: Damon A. H. Teagle and Doug Wilson

1. Introduction

[2] Seismic models that describe magma systems at fast spreading mid-ocean ridges, such as the northern East Pacific Rise (NEPR), envision zones of crystal mush and melt [*Detrick et al.*, 1990; *Sinton and Detrick*, 1992; *Hussenoeder et al.*, 1996; *Singh et al.*, 1998; *Dunn and Toomey*, 2000] similar to the structure of fossil subvolcanic systems [*Marsh*, 2000, 2004]. The volumes of melt in the mush zones are uncertain but likely to vary from ~2% to ~18%, depending on lithostatic load and local tectonics [*Crawford et al.*, 1999; *Crawford and Webb*, 2002].

[3] Melt lenses exist within the crust-mantle transition zone [*Kelemen et al.*, 1997; *Garmany*, 1989; *Boudier et al.*, 1996; *Crawford and Webb*, 2002] and melts accumulate between seismic layer 2 and layer 3 to form an axial magma chamber (AMC) located 1–2 km beneath the ocean floor. Currently, there is debate on whether normal mid-ocean ridge basalt (NMORB) erupts principally from the uppermost melt lens or includes substantial volumes from melt-rich zones within the underlying, stratigraphically high-level crystal mush. In either case, typical NMORB and more chemically evolved compositions develop when primitive melts exit the upper mantle, ascend through the axial magma system [*Korenaga and Kelemen*, 1997, 1998; *Schouten and Kelemen*, 2002] and undergo fractionation and magma mixing [*Langmuir et al.*, 1986; *Dixon et al.*, 1986; *Grove et al.*, 1992; *Perfit et al.*, 1994; *Perfit and Chadwick*, 1998]. (Note: At the NEPR, NMORB is represented by a range of chemical compositions that can largely be explained by mixing of depleted (DMORB) and enriched (EMORB) end-members from off-axis locations, e.g., seamounts.) Several models for the physical stratigraphy of the magma system and the development of lower oceanic crust have been proposed on the premise of a vertical chemical zonation [*Nicolas et al.*, 1987; *Boudier et al.*, 1996; *Natland and Dick*, 1996; *Bédard et al.*, 2000].

[4] The solid products of magmatic processes beneath active ridges are hidden from view so much of the petrologic information regarding growth of oceanic crust comes from ophiolites and gabbros exposed in tectonic windows and detachment zones [*Nicolas*, 1989; *Bédard*, 1993; *Boudier et al.*, 1996; *Macleod et al.*, 1996; *Natland and Dick*, 1996, 2002; *Coogan et al.*, 2000; *Macleod and Yaouancq*, 2000; *Koga et al.*, 2001; *Coogan et al.*, 2002a, 2002b, 2003a, 2003b; *Karson et al.*, 2002; *Dick et al.*, 2002]. These studies support the view that the crustal magma system facilitates chemical refining of ascending melts and metasomatism of the partially solid crust, processes that have been collectively called syntexis [*Bédard and Hébert*, 1996; *Bédard et al.*, 2000]. Isotropic gabbros dominate the upper parts of crustal layer 3, and are quite similar to the chemical array of NMORB erupted at normal MORs [*Coogan et al.*, 2002a]. In contrast, lithologies observed at lower and middle levels of layer 3 do not commonly have equivalent liquid compositions and include a large proportion of cumulates. Many of these cumulate minerals are not in equilibrium with NMORB melts that erupt at the ridge crest, instead they have precipitated from melts that are more primitive [*Kelemen et al.*, 1997]. Here, we describe a melt-rich, olivine-bearing, pyroxene-absent, anorthosite xenolith (presumably a sample of a crystal mush) from the NEPR neovolcanic zone in which evidence for syntexis has been "caught in the act."

[5] The xenolith was included in a relatively primitive NMORB (8.67 wt.% MgO) sheet flow erupted in 1991 within the axial summit trough (AST) at approximately 9°50′N on the NEPR, and subsequently collected in 1994 using Alvin during dive 2737 [*Gregg et al.*, 1993; *Rubin et al.*, 1994; *Fornari et al.*, 1998]. The importance of the xenolith being enclosed in a flow whose eruption date has been precisely dated at 1991 cannot be overstated; the observation indicates that the xenolith is related to the current magmatic system that has been described geophysically [*Detrick et al.*, 1987; *Kent et al.*, 1990, 1993]. This is confirmed by the gross texture, which shows that the xenolith was only partly solidified when captured by the host melt. This is the largest (90 cm^3) example of a similar mineralogical suite of xenoliths we, and others, have collected in young looking, but undated, primitive NMORB lavas along this portion of the ridge. The xenolith reveals important petrologic information about MOR magmatic systems concerning (1) melt distribution in a crystal-dominated mush; (2) melt-crystal reactions within the mush; (3) the chemistry of melts that have contributed to the cumulate lithology; and (4) the chemistry of axial melts that enter the axial magma system.

[6] Several studies document gabbroic xenoliths in samples of NMORB from the active ridge axes of the Juan de Fuca Ridge (JdFR), EPR [*Dixon et al.*,

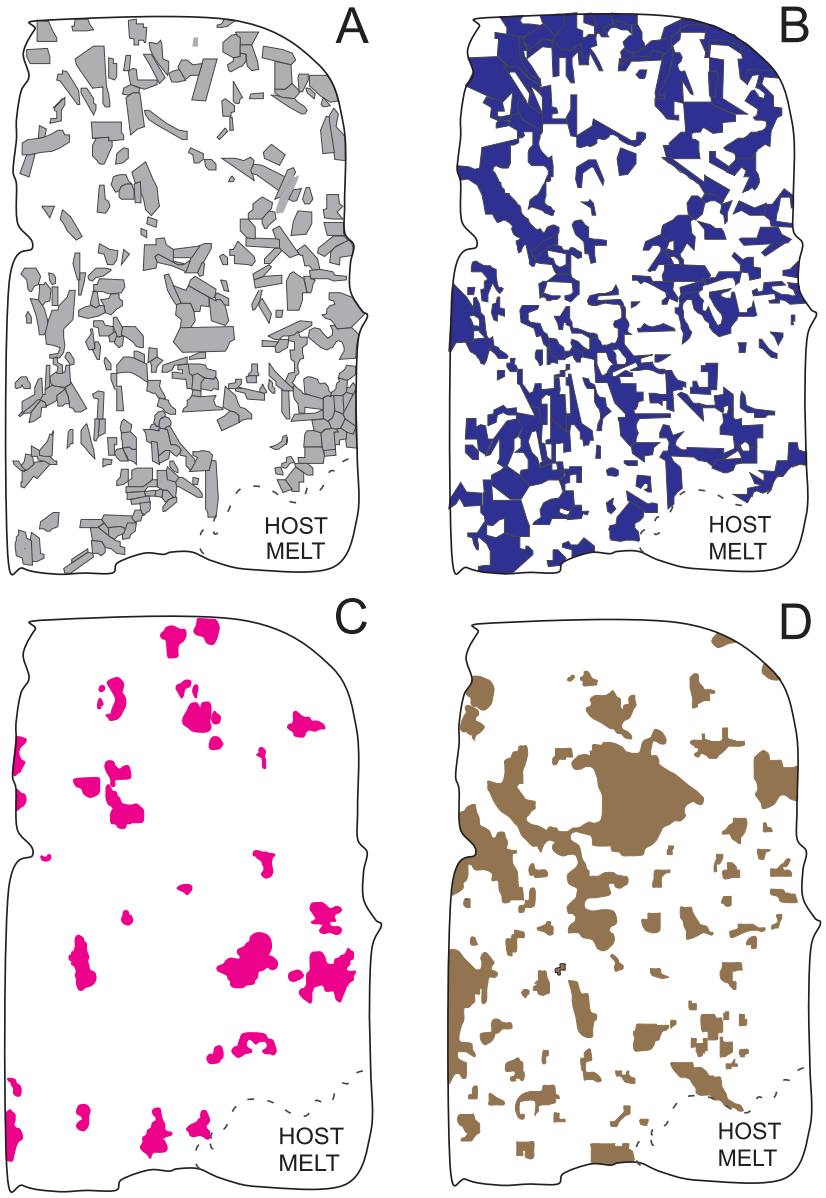

Figure 1. Distribution of phases in the xenolith based on a representative 3-cm-wide petrographic section: (a) Stage 1 plagioclase, (b) Stage 2 plagioclase, (c) olivine, and (d) intergranular glass.

1986; *Hekinian et al.*, 1986; *Davis and Clague*, 1990; *Bender et al.*, 1991; *Smith*, 1993; *Smith et al.*, 1994; *Miller*, 1995] and Iceland [*Gurenko and Sobolev*, 2006]. Most, but not all, recovered xenoliths are medium-grained gabbros, with variable amounts of interstitial glass, enclosed by lavas with <7 wt.% MgO, that is to say, hosted by moderately evolved NMORB. Xenoliths composed of plagioclase + clinopyroxene or plagioclase + olivine are common with minor orthopyroxene, olivine, and titanomagnetite. Most xenoliths have bulk compositions similar to NMORB and their mineralogy and bulk composition suggests they have crystallized from melts that have evolved to the olivine + plagioclase +pyroxene cotectic, although xenoliths with this particular three-phase assemblage are rare. However, based on phase chemistry, minerals within these xenoliths commonly are not in equilibrium with the host melt, i.e., they are not connate inclusions, but may be related to the host melt by in situ fractional crystallization, and mixing. They probably represent fragments of boundary layer mush in varying degrees of solidification [*Dixon et al.*, 1986; *Miller*, 1995] and their evolved NMORB affinities suggest a high stratigraphic level within the developing layer 3 crust.

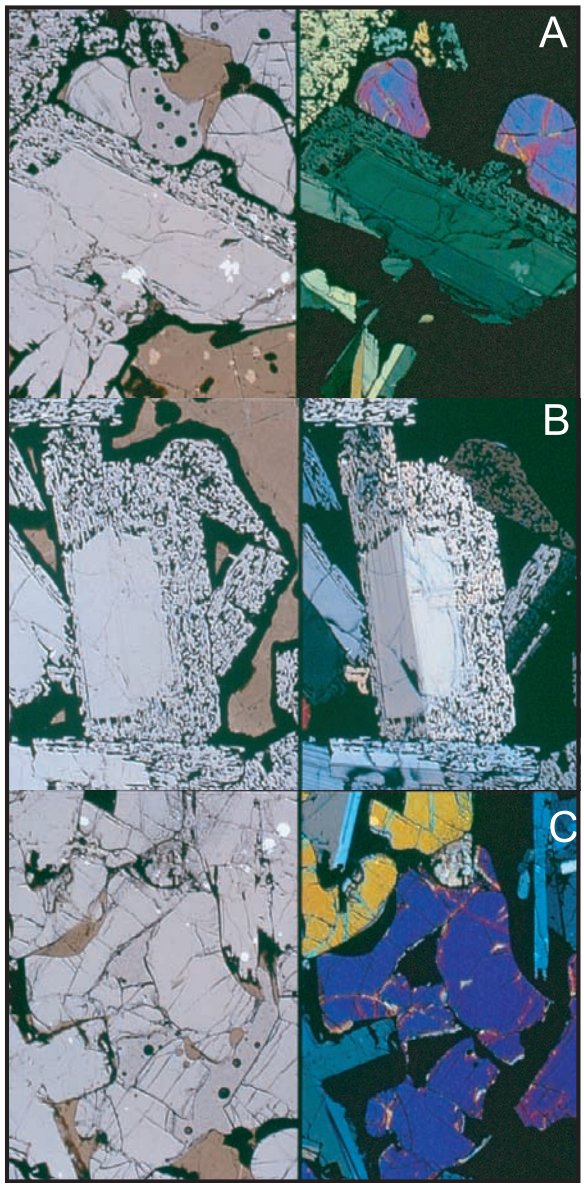

Figure 2. (left) Plain polarized light and (right) cross-polarized light photomicrographs showing textural relations in the xenolith. (a and b) Stage 1 plagioclase cores are mantled by Stage 2 plagioclase displaying a characteristic sieve texture due to dark brown glass inclusions. Note also the distribution of pale brown intergranular glass that has devitrified (black rims) against cumulus plagioclase. Each view is 3 mm wide. (c) Grains of resorbed olivine. View is 5 mm wide.

[7] In contrast to xenoliths that have a clear genetic link to evolved NMORB, two gabbro xenoliths have been described [*Bender et al.*, 1991; *Miller*, 1995] that contain olivine + plagioclase, with ~50% interstitial glass. They were collected during the CHEPR cruise in 1985 at ~9°50′N, and slightly south of the 1991 eruption site. Their mineral chemistry, particularly the presence of very calcic plagioclase, and absence of augite, indicate that they belong to the same lithologic type as the cumulate described here. The fact that several xenoliths with very similar, and unique mineralogy, also contain substantial proportions of intergranular glass adds credence to the notion that they collectively represent fragments of a preexisting crystal mush. Such xenoliths appear to be relatively common within the neovolcanic zone at ~9°50′N, where sampled lavas are more primitive than those to the north or south. This type of xenolith also occurs in more than one lava based upon their collection by the CHEPR cruise in 1985 prior to the eruption of the 1991 flow [*Bender et al.*, 1991], frequent recovery of small xenoliths in lavas along the axis in the 9°37′ to 9°53′N section of the EPR during cruises from 1991 to 2000 [*Smith et al.*, 1994], and recovery of similar xenoliths from undated lava during the 2006 Atlantis cruise to examine the recent eruption on the EPR near 9°50′N (M. Perfit, K. Rubin, and S. A. Soule, unpublished data, 2006).

2. Texture and Phase Chemistry

[8] The xenolith is a matrix-dominated, cumulate olivine anorthosite (using the IUGS terminology of *Le Maitre* [1989]), composed of anorthite (An_{94-90}) and labradorite (An_{90-70}), intergranular olivine ($Fo_{86\pm0.3}$) and glass, with minor sulfide and spinel. The xenolith collected in NMORB sample 2737-3 has a volume of ~90cm^3 and is surrounded by glass quenched from the host lava. Small vesicles (up to ~2 mm) are concentrated along the edge of the xenolith in some places. Figure 1 maps the distribution of the individual major phases based on a representative photomicrograph. The crystal mode, calculated from 1000 points in each of three thin sections, is ~70% plagioclase, ~9% olivine, ~21% intergranular glass, with minor (<0.2%) sulfide and spinel. Clinopyroxene is absent. An interconnected network of plagioclase crystals defines the cumulate texture (Figures 1a, 1b, and Figure 2). The plagioclase to olivine modal ratio is ~7:1 far different from the modal proportions expected to crystallize from NMORB (~2:1).

2.1. Plagioclase

[9] The network of plagioclase crystals comprises euhedral, subhedral, equant and tabular grains with an average size of 3 mm. Individual crystals can be divided into core (Stage 1) and mantle (Stage 2) based on the absence of glass inclusions in the

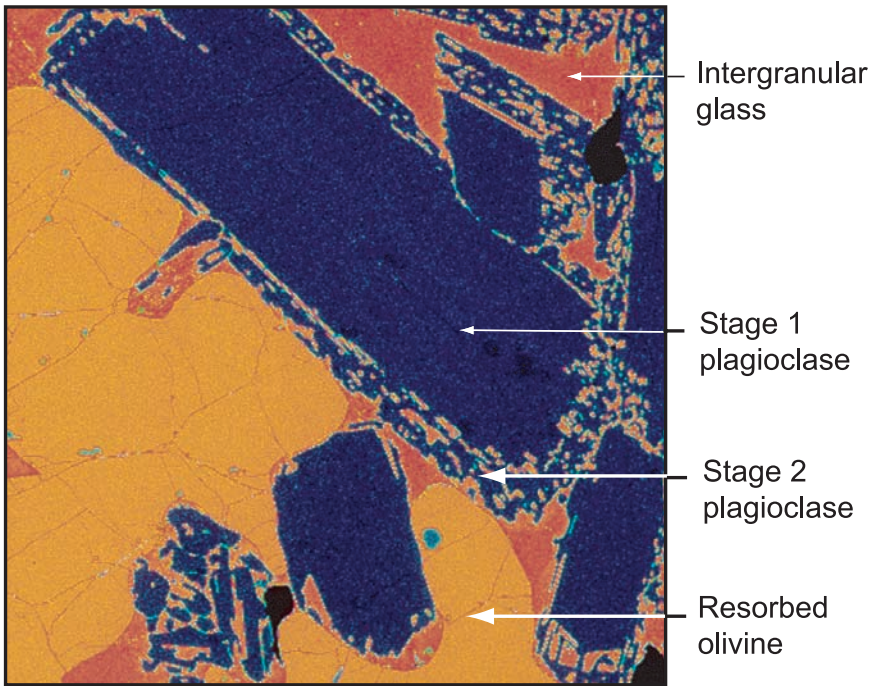

Figure 3. Backscatter electron image in false color showing the texture of the xenolith. The brighter colors represent higher mean atomic weight. Note the partial engulfing of plagioclase (dark blue) by olivine (yellow) at the bottom of the image. Intergranular glass and glass inclusions in Stage 2 plagioclase are shown in orange.

former and abundance of glass inclusions in the latter (Figures 1a, 1b, 2, and 3). Core plagioclase (An_{94-90}) has a narrow rim with several compositional reversals from An_{90} to An_{86}. A convoluted resorption surface crosscuts the compositional reversals (Figure 4) and separates core from mantle. The mantles also have crenulate margins (Figures 3 and 4).

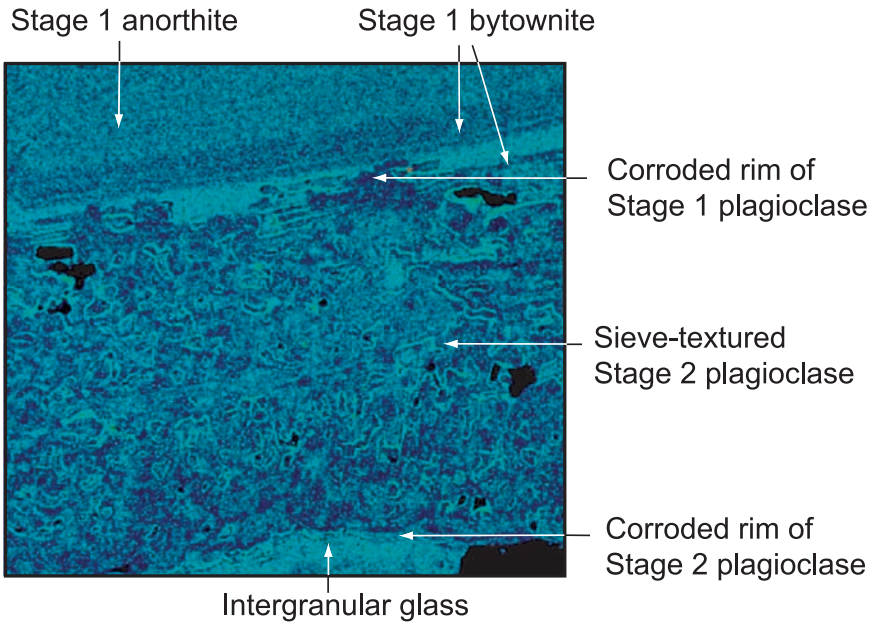

Figure 4. Details of the boundary between Stage 1 and Stage 2 plagioclase shown in a false color Na X-ray image. Note the oscillatory zoning at the margins of Stage 1, the crenulate resorption surface between the plagioclase growth stages, and the patchy zoning in Stage 2 plagioclase.

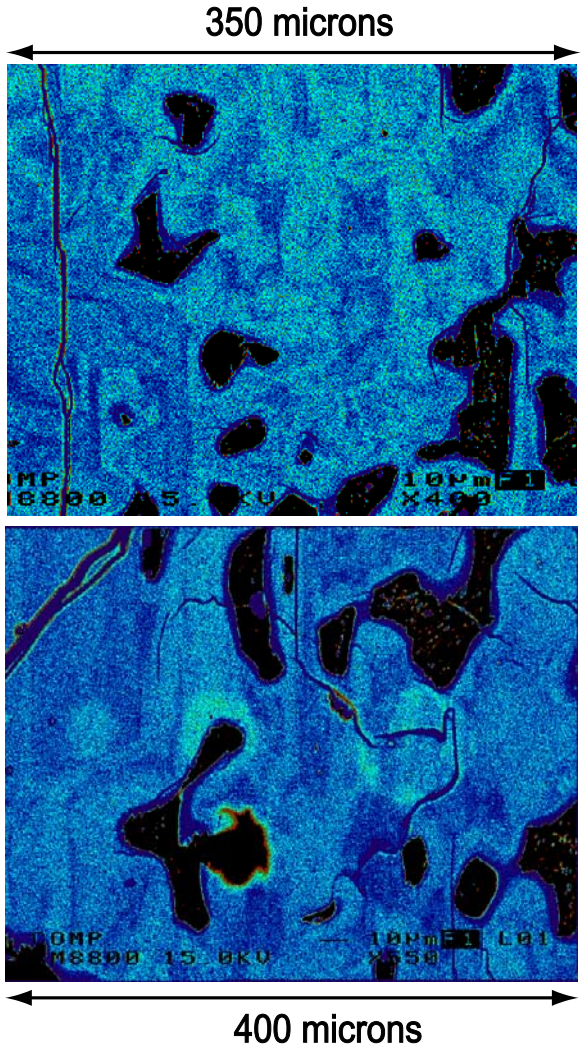

Figure 5. Na X-ray image, using the X-ray mapping capabilities of the JOEL JXA 8800L electron microprobe, presented in false color, showing details of the patchy zoning in Stage 2 plagioclase. The lighter colors indicate relative Na enrichment. The black areas are glass inclusions. The texture is now diffuse due to the percolation of later melts that facilitated Na metasomatism of Stage 2 anorthite to bytownite and loss of some porosity due to bytownite precipitation in pore spaces. The process of syntexis was arrested when the xenolith was captured. The distribution of glass inclusions (yellow outlines) defines the sieve texture and reflects the contemporaneous porosity that was filled by melt just prior to the capture of the xenolith.

[10] Stage 1 plagioclase is represented by the cores of cumulate plagioclase. It involved precipitation, and accumulation of anorthite – bytownite crystals followed by partial resorption. The original degree of compositional variability in Stage 1 plagioclase cannot be determined because of resorption. Every Stage 1 plagioclase crystal is surrounded by a resorption surface allowing the modal distribution of Stage 1 grains to be mapped (Figure 1a) and indicating that prior to the precipitation of Stage 2 plagioclase the cumulate was melt-dominated, composed of ~40% crystals and ~60% melt. The sieve-textured mantles represent Stage 2 growth of plagioclase followed by a further period of partial resorption. The mantles comprise approximately 50 modal percent of the total plagioclase (Figure 1b) or 80%–90% of the total volume of cumulate plagioclase. The compositional zoning in the Stage 2 plagioclase is highly complex compared to the simple zoning patterns observed in Stage 1 plagioclase. The Stage 2 plagioclase exhibits a distinct patchy zoning that represents a pattern of secondary compositional variability (see below) that has been superimposed upon the original Stage 2 plagioclase zoning.

[11] A ubiquitous feature of Stage 2 plagioclase is a moth-eaten appearance (“sieve texture”) because of inclusions of dark brown glass (Figures 2 and 3). The glass inclusions represent the distribution of melt filled pores within the Stage 2 plagioclase at the time the xenolith was captured. The shapes of the individual patches that collectively define the patchy zoning mimic those of the glass inclusions (Figure 5).

[12] Microprobe data indicate that Stage 1 plagioclase crystallization was initiated by precipitation of anorthite followed by bytownite (Figure 6, Auxiliary Material[1] Table S1). The Stage 2 plagioclase also includes patches that have anorthite composition but includes a larger proportion of bytownite than the Stage 1 plagioclase. The chemical zoning is substantially more complex in Stage 2 (Figures 7 and 8,Tables S2 and S3). The areas of patchy zoning contain “islands” of anorthite (Figure 7) that have a sharp outline with the surrounding bytownite. However, the majority of the areas of patchy zoning are devoid of anorthite and show sharp compositional oscillations between sodic and calcic bytownite (Figure 8, traverses A → B and C → D) and areas that are relatively unzoned (Figure 8, traverse E → F). In Stage 1 plagioclase the MgO concentrations increase with decreasing anorthite content (Figure 9, Table S4). Generally, this relation is consistent with the var-

[1]Auxiliary materials are available at ftp://ftp.agu.org/apend/gc/2006gc001316.

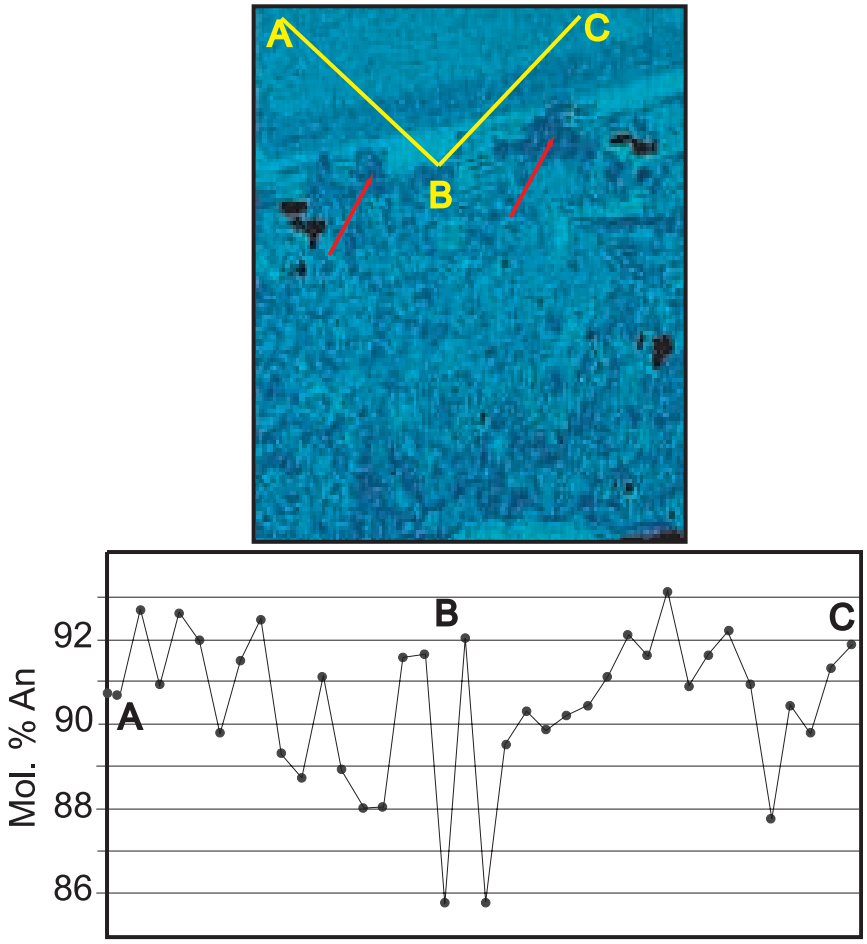

Figure 6. Compositional variations within Stage 1 plagioclase expressed as mole% anorthite. See Table S1 for details of analytical technique. The traverse A-B-C is shown in the false color Na X-ray image at top (also Figure 3) but does not include the complete core region, which shows compositional oscillations between An_{94} and An_{90}. Toward the crenulate resorption surface (red arrows), which defines the boundary between Stage 1 and Stage 2 plagioclase, the Stage 1 plagioclase gradually zones to An_{88} and then to An_{86} at the resorption boundary. This suggests that the Stage 1 plagioclase lost to resorption was principally bytownite. The plagioclase compositions are in Table S1.

iation in $K_{MgO}^{plag/melt}$ but a more detailed evaluation of crystal residence times [*Costa et al.*, 2003] is precluded because of resorbed plagioclase.

2.2. Olivine

[13] Olivine grains vary from 1 mm to 3 mm in size (Figure 1c), are rounded and embayed (Figure 10, Table S5) and contain round and ovoid melt inclusions. The latter are discussed below. Most grains show minor normal zoning, less than 1 mole percent forsterite (Figure 10), with a composition close to Fo_{86}. However, a few grains show very minor reverse zoning. Ca contents average ~2300 ppm with no appreciable zoning (±100 ppm) from core to rim.

2.3. Glass

[14] Four different types of glass are present within, or associated with, the xenolith: (1) light brown host glass attached to the rim of the xenolith; (2) intergranular light brown glass within the solid crystalline matrix; (3) round and ovoid light brown melt inclusions in olivine; and (4) dark brown glass inclusions in Stage 2 plagioclase mantles.

2.3.1. Host Glass

[15] Host glass surrounds the xenolith. It is separated from the xenolith by a disconnected narrow rim where the host melt has quenched to a microcrystalline aggregate. Where the latter is in contact

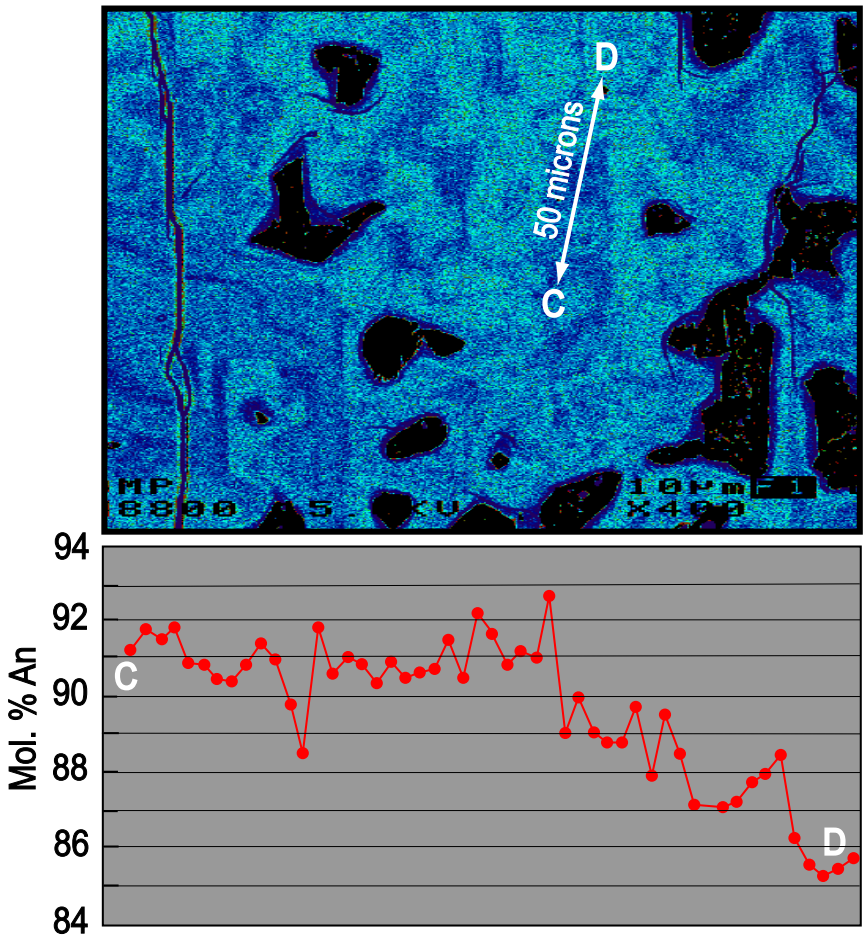

Figure 7. A detailed microprobe traverse through the Stage 2 patchy zoned plagioclase. The traverse is shown on the false color Na X-ray image at top. Note that this particular traverse demonstrated unequivocally that anorthite crystallized as part of the Stage 2 assemblage. The plagioclase compositions are in Table S2.

with xenolith intergranular glass the contact is sharp. The host glass composition (Table S9) is a relatively primitive NMORB with Mg# (molar Mg/Mg + Fe^{2+}) = 0.63 ± 0.05, MgO = 8.6 ± 0.1 wt.%, molar Ca/Na = 5.3.

2.3.2. Intergranular Glass

[16] Intergranular glass is pale brown, chemically homogeneous primitive NMORB. The intergranular glass has Mg# = 0.61 ± 0.05, MgO = 8.23 ± 0.1 wt.%, molar Ca/Na = 4.9. This is the most evolved of all the glass types, although only marginally so relative to the host melt. It represents the melt occupying intergranular pores within the anorthosite cumulate when the xenolith was captured. Dark devitrified glass is ubiquitous at the contacts between intergranular glass and the crystalline matrix and has a composition identical to the pale brown glass.

[17] The intergranular porosity, as defined by glass-filled pores, has a volume of ~21% and has a bimodal size distribution. Twenty-five percent of the glass-filled pores are within the size range 0.50 to 0.23 mm^2 and the remaining 75% have a mean size of 0.08 mm^2 with a standard deviation of 0.03 mm^2 (Figure 11). Connectivity between the largest patches of glass (macropermeability) is through irregular tubular and planar channels (Figure 1d). Grain boundary connectivity between many of the smaller pores (micropermeability) occurs as thin grain boundary films. As the pores decrease in size to ~0.02 mm. they become isolated and these pores represent ~20% of the total porosity. Thus ~80% of the porosity was connected, potentially facilitating intergranu-

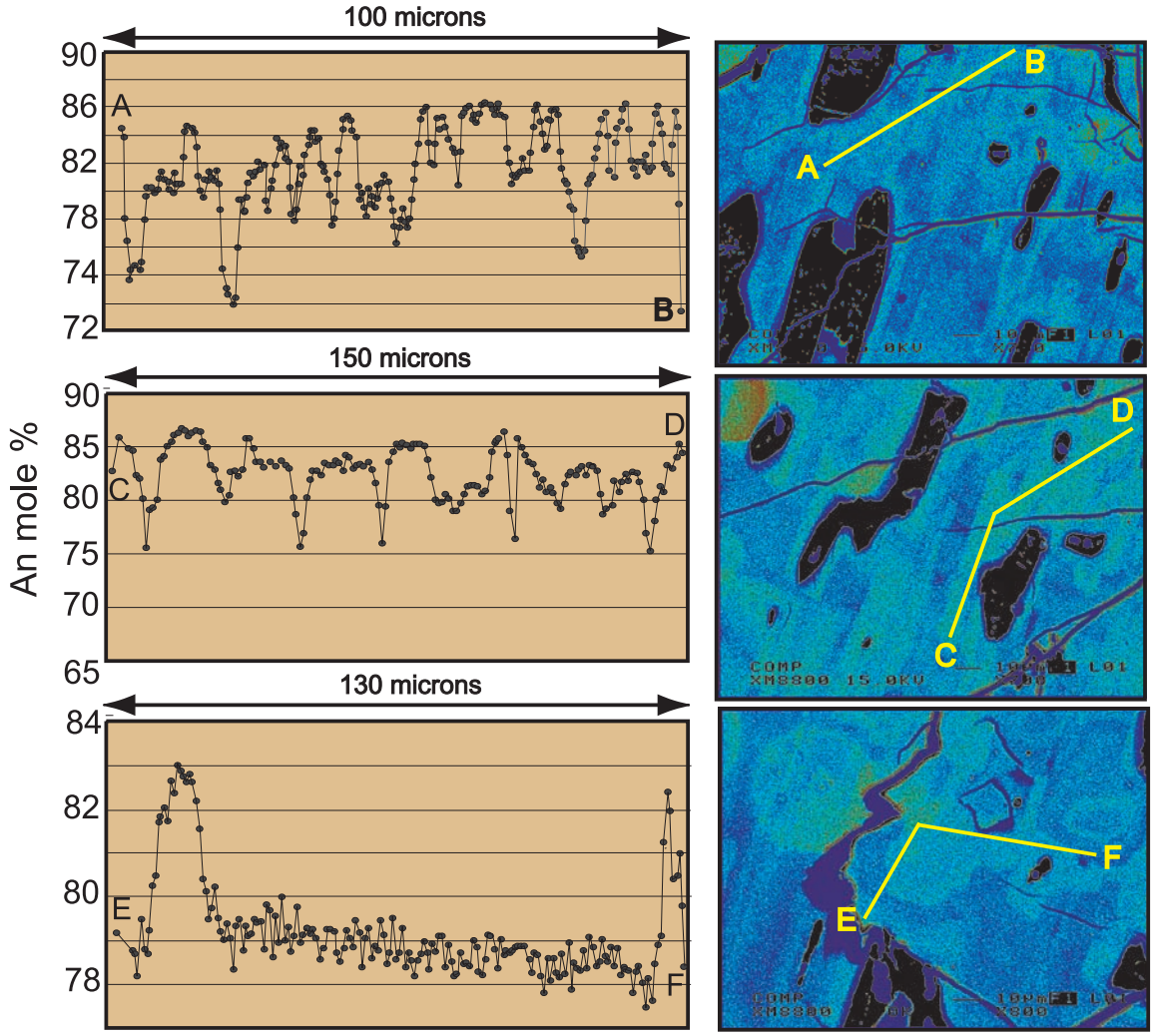

Figure 8. Compositional variations across complexly zoned patchy zones in Stage 2 plagioclase. The location of each traverse is shown in the false color Na X-ray images to the right. These traverses include areas that show oscillatory structure and areas almost devoid of zoning. Such complexity probably arises through syntectic reactions whereby the plagioclase zoning results from metasomatism and precipitation from local melt in channels within the Stage 2 latticework that have limited chemical communication with intergranular melt. The overall range of zoning in Stage 2 plagioclase is from An_{93} to An_{78} (Figure 7). The plagioclase compositions are in Table S3.

lar movement of melt. An estimate of connectivity between ~80% of pore space, i.e., ~17% total porosity, is consistent (perhaps fortuitously so) with recent seafloor compliance measurements [*Crawford and Webb*, 2002] that indicate, on average, porosity within the mush zone beneath the crest of the EPR at ~9°50′N is ~17%.

2.3.3. Olivine Melt Inclusions

[18] Crystal-free glass inclusions in olivine have variable compositions due to postentrapment crystallization of the host olivine (Fo_{86}) at the original melt inclusion boundaries. Detailed probe traverses toward and across inclusion boundaries indicate that the largest inclusions (~300μ in diameter) have slightly Fe-enriched diffusion rims (<2 mol% Fo) that are ~10μ to 15μ wide. These rims become progressively less wide as the inclusion sizes decrease. The diffusion profiles indicate a loss of FeO from the inclusions of less than 0.1 wt.%, close to the normal precision for FeO by microprobe. Thus we consider that the melt inclusions have not been severely compromised by postentrapment diffusion [*Danyushevsky*, 2001]. For each inclusion the chemistry of the original melt was resurrected by reverse fractionation into the modified glass compositions until the glass was in equilibrium with Fo_{86}. The average $K_{Mg/Fe}^{Fo/melt}$

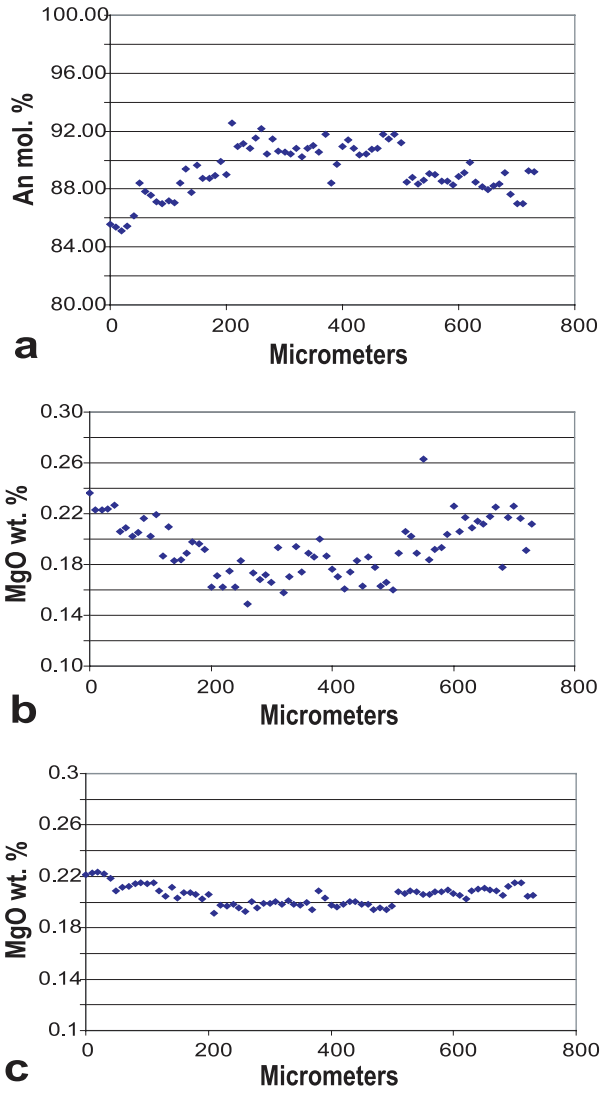

Figure 9. Compositional profile across a Stage 1 plagioclase showing the relation between (a) An content and (b) MgO content. (c) The equilibrium profile (see text for discussion) based on equation (3) of *Costa et al.* [2003]. The plagioclase compositions are in Table S4.

during this exercise was 0.31 and produced a suite of melt inclusions with Mg# ~0.66.The amount of olivine added to the inclusions, i.e., the amount of olivine precipitated on the walls of the inclusions, varies from 5.2% to 13.5% (Table S5).

[19] Major element plots indicate two main inclusion populations (Figure 12, Table S5). The two types can be separated into low TiO_2 (Type 1) and high TiO_2 (Type 2) groups. They have similar MgO values but the Type 1 inclusions have lower Na_2O and K_2O, and higher Ca/Na and Ca/Al ratios. The type 1 inclusions can also be divided into subgroups 1a and 1b. The latter have higher MgO, FeO, and a slightly higher Ca/Al ratio (Table S5). The type 1 inclusions have Ca/Al ratios similar to the host glass and intergranular glass but the Type 2 inclusions have lower ratios and higher TiO2 and Na_2O contents. Both Type 1 and Type 2 inclusions are more primitive than either the host or intergranular glasses.

2.3.4. Glass Inclusions in Plagioclase

[20] Glass inclusions in plagioclase are very abundant. They are dark brown colored, irregularly shaped and define the sieve texture of the plagioclase mantles. Channels of glass connect individual inclusions toward the outermost part of the sieved mantle, whereas inward the inclusions are isolated. Where the outermost inclusions are in contact with intergranular glass the contact is sharp.

[21] Glass inclusions in plagioclase have a wide range of major element chemistry (Figure 13, Table S7) and have neither basaltic nor plagioclase melt compositions. Their compositions form linear correlations between Al_2O_3, MgO, CaO, and FeO, but no correlation between Al_2O_3 and Na_2O. A few of the melt inclusions overlap the compositions of the olivine melt inclusions and the intergranular glass, but they are generally distinct from either of these glass compositions. Many of the inclusions are rimmed by bytownite of $\sim An_{80}$ composition (for instance, the rims around the melt inclusions in Figure 5).

2.4. Spinel

[22] Inclusions of slightly zoned aluminous chromite are found in Stage 1 plagioclase and within the intergranular glass (Table S6). Spinels enclosed within plagioclase have a higher Mg# ($Mg^{2+}/Mg^{2+} + Fe^{2+}$) values of 0.77 to 0.73 compared to spinels within the intergranular glass (0.65 to 0.6), lower Cr# ($Cr^{3+}/Cr^{3+} + Al^{3+}$) values of 0.42 to 0.41 than those in glass (0.59 to 0.56), slightly higher Fe# ($Fe^{3+}/Fe^{3+} + Cr^{3+} + Al^{3+}$) values of 0.13 to 0.12 versus 0.11 to 0.07, and lower Fe^{2+}/Fe^{3+} ratios.

2.5. Sulfide

[23] Droplets of sulfide, up to 1.5 mm in diameter, are attached to the outer edge of the xenolith and are partially surrounded by the host glass. Sulfide blebs from 50 to 200 microns are also observed within the Stage 1 plagioclase and submillimeter sulfide blebs are also found within the intergranular glass (Figure 14). No large sulfide droplets were

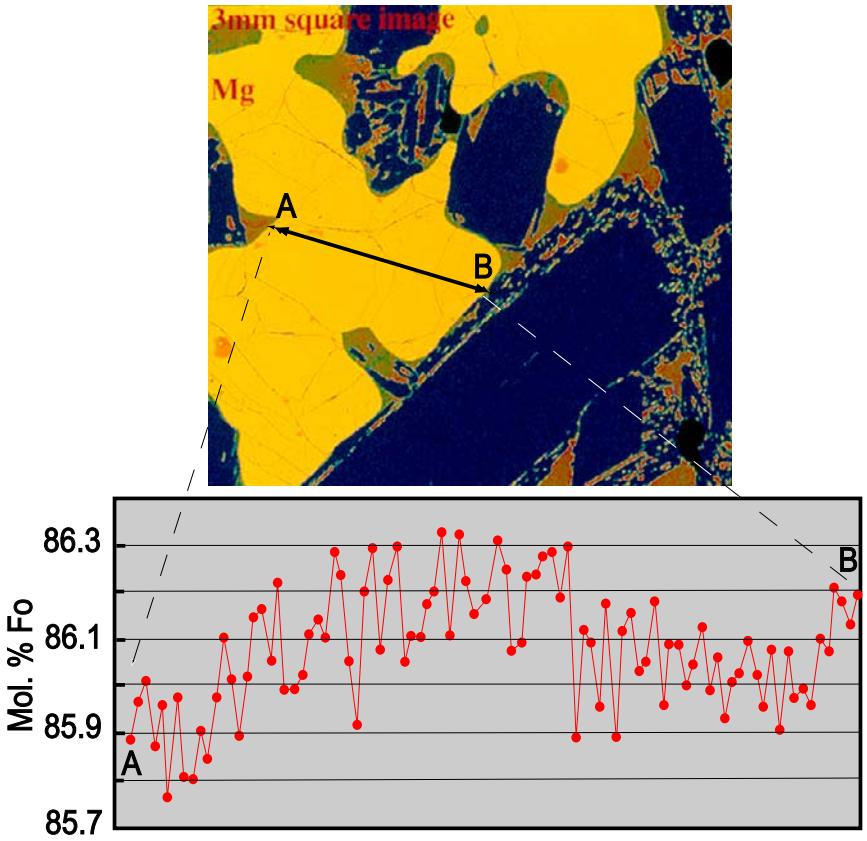

Figure 10. Compositional variation across an embayed olivine grain. The location of the traverse is shown on the false color backscatter image at top. Note the growth of olivine (yellow) around cumulate plagioclase (blue). The normal zoning pattern, although very slight, is typical of most olivine grains, but a few show equally subtle reverse zoning. The olivine compositions are in Table S5.

found completely enclosed within the xenolith. The margins of the large droplets that are in contact with the host lava are crunulate and resorbed, whereas the contacts with intergranular melt at the xenolith edges are smooth.

[24] All sulfides have crystallized to a three-phase assemblage (Figure 14, Table S8) with initial, precipitation of a compositionally uniform Fe-Ni-S monosulfide solid solution. This accounts for ~85% of the solidification before the appearance of a compositionally uniform Fe-Ni-Cu-S intermediate solid solution (iss). The latter phase accounts for the remaining 15% of solidification together with a small proportion of interstitial iron oxide. The sulfide blebs in the intergranular glass only rarely contain the iss phase and some show a slight increase in Cu toward the rims (Table S8). Both the monosulfide phase and iss phase are well developed in the large droplets. The marginal corrosion of sulfide by the host melt has resulted in a preferential dissolution of the iron oxide and iss phases resulting in a spongy texture.

3. Discussion

3.1. Stage 1 Plagioclase

3.1.1. Melt Source

[25] NMORB is the dominant magma series that constructs the NEPR uppermost crust, based on the compositional distribution of lavas erupted at the ridge crest [*Langmuir et al.*, 1986; *Batiza and Niu*, 1992; *Perfit et al.*, 1994; *Perfit and Chadwick*, 1998; *Smith et al.*, 2001]. The MgO contents of NEPR NMORB range from approximately 6 wt.% to 10 wt.%, but the dominant lavas type has an MgO content less than 8 wt.% (Figure 15). Observations from NMORB lavas that have crystallized plagioclase and phase equilibrium considerations indicate that NMORB lavas that are nearly anhy-

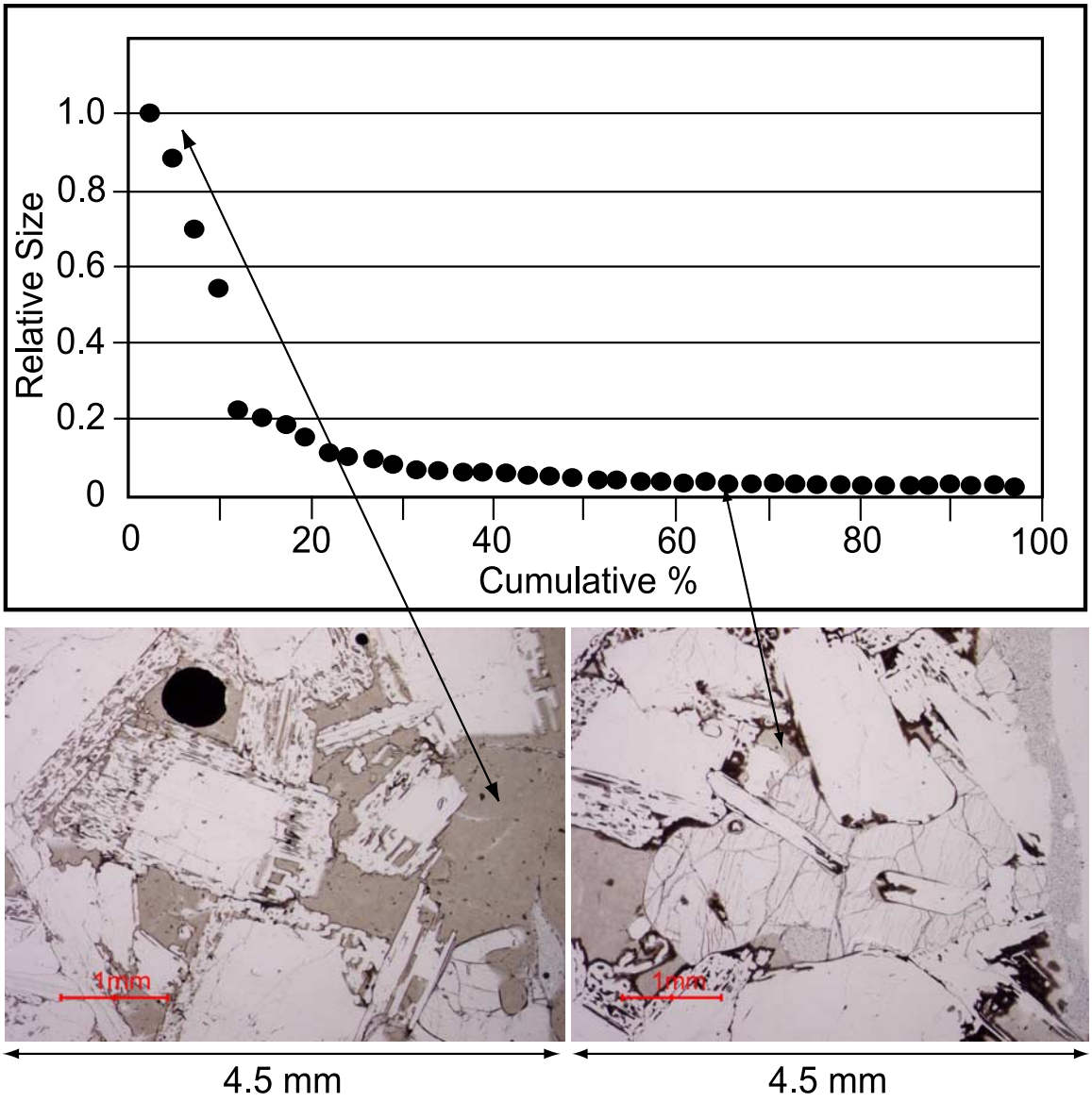

Figure 11. Distribution of intergranular melt based on point counting of three petrographic thin sections (1000 points/thin section). Note the bimodal distribution of pore space. Visual representation of the larger pores is shown at the bottom left, and visual representation of the small pores is shown at the bottom right. The larger pores form a permeable network, whereas the very small pores are isolated and do not contribute to the matrix permeability.

drous do not crystallize anorthite-bytownite plagioclase. Primitive NMORB melts have molar Ca/Na ratios that are too low to crystallize anorthite under equilibrium or near-equilibrium and this is illustrated by the absence of highly calcic plagioclase phenocrysts in NMORB lavas. Consequently, the common presence of anorthite-bytownite xenocrysts in erupted NMORB lavas [*Sinton et al.*, 1993; *Nielsen et al.*, 1995; *Pan and Batiza*, 2003] and anorthite-bytownite cumulates in ophiolites is enigmatic. Similarly, the cumulate described here contains a significant amount of anorthite, particularly as a cumulate phase during the Stage 1 precipitation of plagioclase. This phase cannot have crystallized from any of the moderately primitive melts that have been identified within the cumulate because they have Ca/Na ratios that would be expected to precipitate sodic bytownite or labradorite (Figure 16).

[26] Precipitation of anorthite can occur by Na diffusion between melts with extremely different

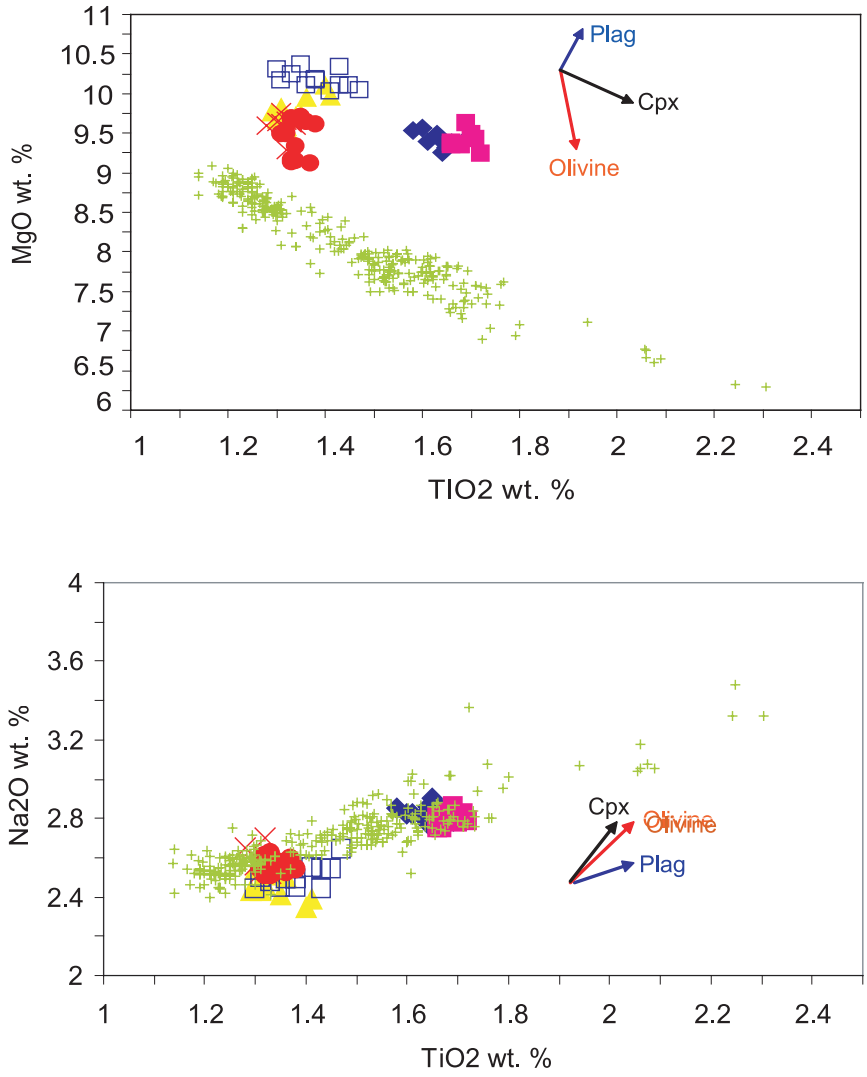

Figure 12. Plots of MgO and Na_2O versus TiO_2 for melt inclusions in olivine. The inclusions form two populations that can be separated on TiO_2 content with Type 1 having lower TiO_2 than Type 2 (solid red squares and solid blue diamonds). Type 1 may also be further divided into Type 1a (solid red circles, red crosses, yellow triangles) and 1b (open blue squares) on the basis of MgO content. Vectors are also shown for removal or addition of olivine (red), plagioclase (blue), and clinopyroxene (black). The compositional field of EPR NMORB between 9°N and 10°N is based on over 1200 basaltic glass analyses (M. R. Perfit et al., High-resolution geochemical data set from the East Pacific Rise crest 9°17′N to 10°N: Integrated magmatic and volcanic processes at a fast spreading mid-ocean ridge, manuscript in preparation, 2006; hereinafter referred to as Perfit et al., manuscript in preparation, 2006). The olivine melt inclusion compositions are in Table S5.

Ca/Na ratios [*Lundstrom et al.*, 2005], but this is an unlikely process, or at least a very minor process, in a ridge environment dominated by basaltic melts with similar Ca/Na ratios. It seems unlikely that a plagioclase cumulate could form under circumstances that were substantially removed from the equilibrium condition, given the implication of relatively slow cooling. In addition, the ubiquitous low water content of fresh NMORB lavas suggests that high partial pressure of water that would move plagioclase equilibrium toward more calcic compositions is an unlikely condition for the crystallization of basaltic melts beneath ridges, and thus cannot have contributed to the precipitation of highly calcic plagioclase. A reasonable explanation for the presence of anorthite is that it simply reflects an unusually high melt Ca/Na ratio. Phase equilibrium constraints indicate that in dry systems anorthite crystallizes from silicate melts with molar Ca/Na ratios greater than ~11.5 at the plagioclase

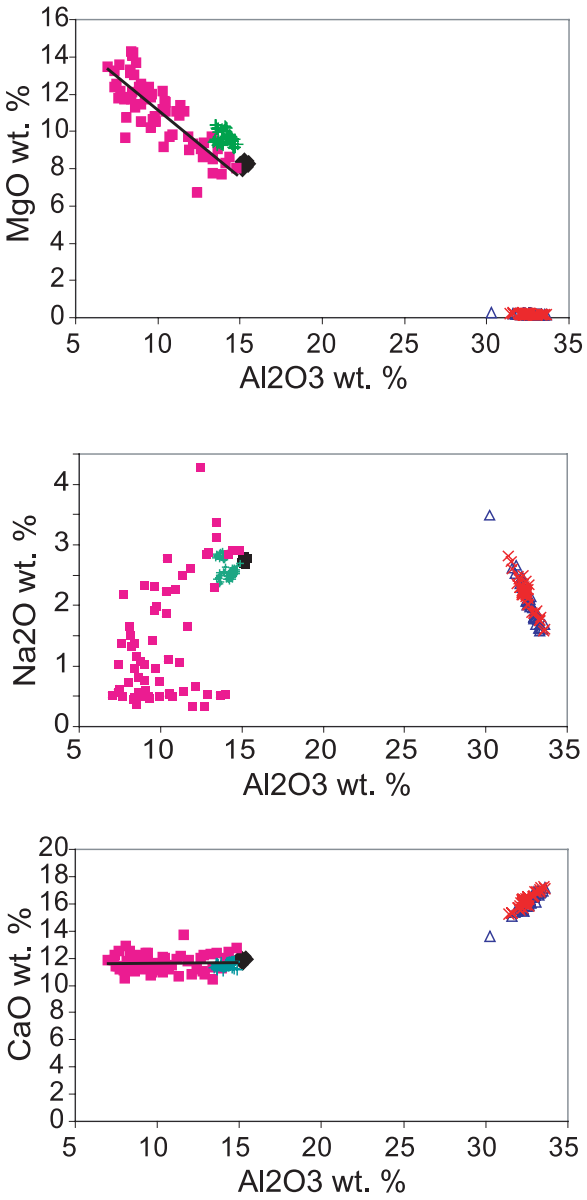

Figure 13. Plot of MgO, Na_2O, and CaO versus Al_2O_3 for glass inclusions (purple squares) in Stage 2 plagioclase. The inclusions fall marginally into the fields of the intergranular glass (black diamonds) and the melt inclusions in olivine (green crosses). The compositions of Stage 1 plagioclase (red crosses) and Stage 2 plagioclase (blue open triangles) are also shown. The glass inclusions and plagioclase data are in Table S7, and the olivine melt inclusion data are in Table S5.

liquidus. Such melts cannot be directly related to primitive NMORB because the liquid line of descent is dominated by the initial precipitation of olivine, which will not move the melt Ca/Na ratio to the lower values observed in primitive, olivine-saturated NMORB (Figure 16). Even the precipitation of clinopyroxene and olivine will not be sufficient to achieve the low Ca/Na ratios observed in NMORB. That is, the cumulate xenolith described here indirectly indicates the presence of melts beneath the NEPR that are distinct from, and not part of, the common NMORB lineage. The question then remains, how can melts with high Ca/Na ratios be produced?

[27] Important considerations in determining the melt Ca/Na ratio are source composition, mineralogy, and degree of melting (temperature). In three-phase lherzholite compositions the activities of calcium and sodium in the melt phase are buffered by the reaction: $CaO^{melt} + 2NaAlSi_2O_6^{cpx} + 3Mg2SiO_4^{ol} \leftrightarrow Na_2O^{melt} + CaAl_2SiO_6^{cpx} + 6MgSiO_3^{opx}$ as long as all of the solid components remain in the mantle assemblage. However, melting depletes the sodium Tschermaks component so that melting of mantle depleted by previous melting events will produce melts with higher Ca/Na ratios compared to more fertile sources. Thus melts with abnormally high Ca/Na ratios could potentially be produced by partial melting of mantle regions that are more depleted than NMORB sources. Experimental melts with Ca/Na ratios ~11.5 can be produced by batch melting at 25 kb, near the spinel-garnet peridotite phase transition [*Elthon and Scarfe*, 1984; *Falloon et al.*, 1998] (Figure 16). These melts are highly magnesian (>15 wt.% MgO), have high liquidus temperatures (~1380°C), low viscosities (<100 poise) and undergo a protracted period of olivine crystallization during ascent through the upper mantle prior to the crystallization of anorthite and calcic bytownite at lower crustal pressures.

[28] The extent to which these batch melts contribute to the melt budget beneath ridges is debatable, given the current understanding of mantle dynamics beneath ridges that suggests polybaric melting is a more likely process. *Kinzler and Grove* [1992] and *Kinzler* [1997] have used equations parameterized from melting experiments to show that accumulation of polybaric fractional melts can reproduce the compositional spectrum of primitive NMORB lavas with relatively low Ca/Na ratios. These results are consistent with the presence of a column of mantle beneath ridges from which melt is extracted and collected near the crust-mantle boundary. However, polybaric melting also provides favorable conditions for development of melts from depleted mantle sources [*Jagoutz et*

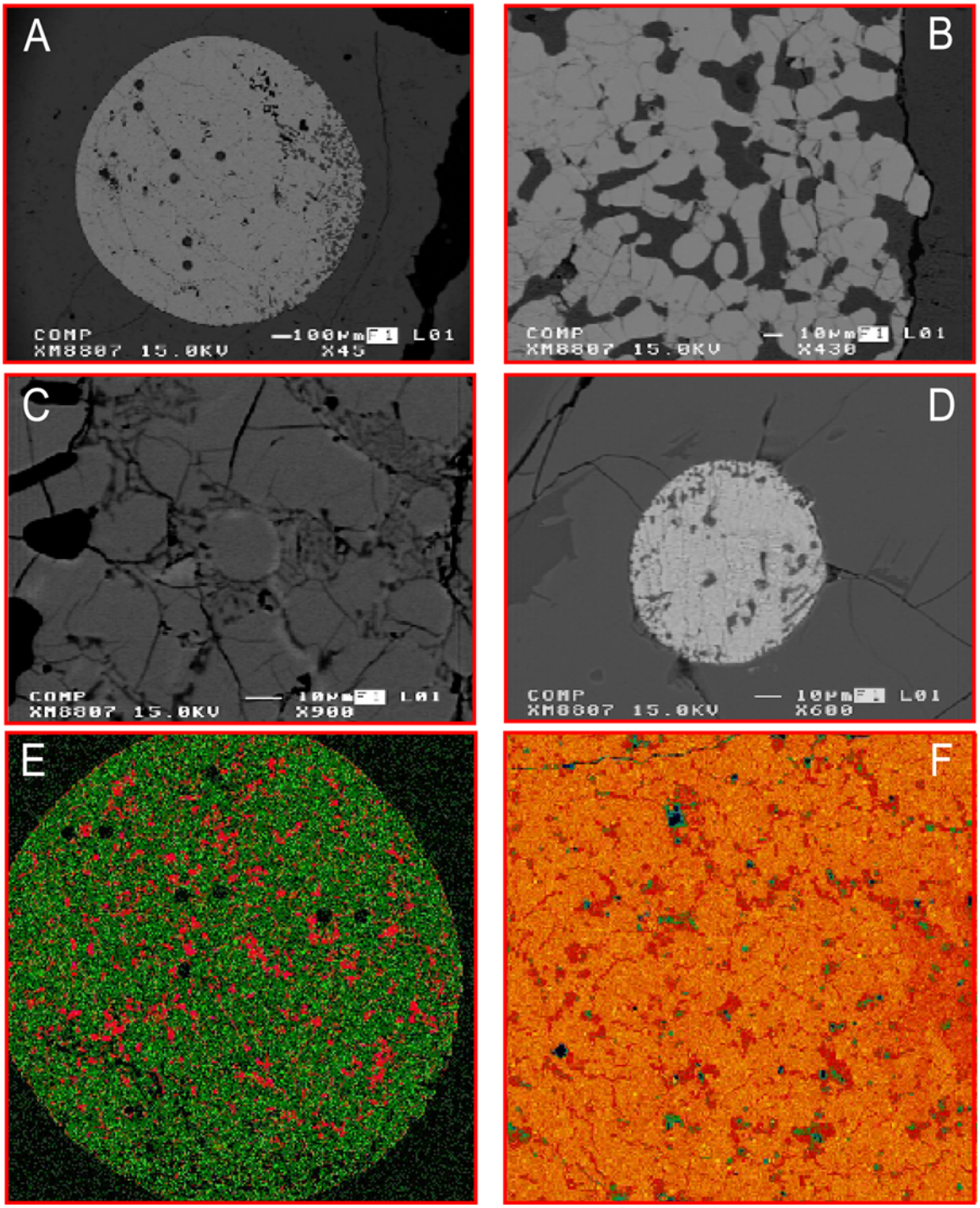

Figure 14. Sulfide droplets associated with the xenolith. (a) Secondary electron image of a 1.4 mm droplet attached to the outer surface of the xenolith (left). The droplet shows a crunulate contact with the host glass (right). (b) Details of the crenulated sulfide surface in contact with host glass. (c) Backscatter electron image of the interior of a sulfide droplet showing details of the compositional variability. The major phase (medium gray) is a Fe-Ni monosulfide rimmed by a Ni-Cu solid solution (light gray). The interstices are filled with iron oxide. (d) Secondary electron image of an 80-micron sulfide bleb within the interior of the xenolith. (e) False color X-ray image of a 15 mm droplet showing the distribution of Cu. The red color indicates the distribution of the Ni-Cu solid solution; the green represents the F-Ni monosulfide. (f) A false color X-ray image showing the distribution of Fe within a sulfide droplet. The green is the Ni-Cu solid solution, medium orange is the Fe-Ni monosulfide, and the dark orange is the interstitial iron oxide phase. Sulfide composition data and analytical techniques are shown in Table S8.

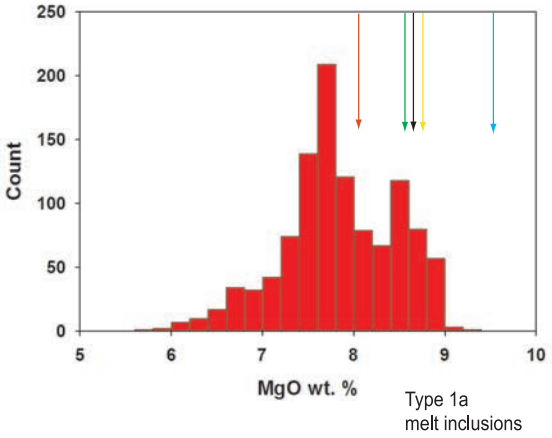

Figure 15. Histogram of MgO wt.% values for NMORB glasses from the NEPR between 9°N and 10°N, based on approximately 1200 analyses of basaltic glasses (Perfit et al., manuscript in preparation, 2006). Also shown are the MgO wt.% values for the xenolith host melt (green arrow), intergranular melt (red arrow), and melt inclusions (Type 1a, yellow arrow; Type 1b, blue arrow; Type 2, purple arrow).

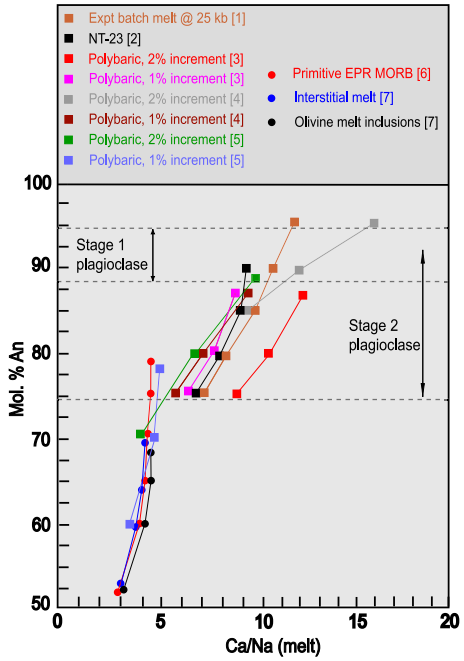

Figure 16. Fractional crystallization of a variety of basaltic melt compositions relevant to the evolution of NMORB and the cumulate xenolith expressed as variations in melt Ca/Na ratios and plagioclase compositions. The trends begin with the first appearance of plagioclase based on fractional crystallization models. The melts include model and natural compositions. All of the melts initially precipitated olivine prior to the appearance of plagioclase. The models were calculated at 3 kb pressure using the program PETROLOG [*Danyushevsky*, 2001] using the following mineral-melt equilibrium data: olivine, *Ford et al.*, [1983]; plagioclase, *Danyushevsky* [2001]; clinopyroxene, *Danyushevsky et al.*, [1996]. Melt ferrous/ferric ratios were calculated at QFM-1 log units using the model of *Borisov and Shapkin* [1990]. The starting basaltic melt compositions are as follows. [1] The experimental batch melts, produced at 25 kb by *Falloon et al.* [1998], also described as a precursor to MORB. [2] An aphyric picrite, NT23, from the Tortuga ophiolite, Chile, that *Elthon* [1979] and *Elthon and Scarfe* [1984] consider to be a primitive precursor to MORB. [3] 1%/km and 2%/km fractional melts produced by partial melting of the depleted mantle composition of *Jagoutz et al.* [1979]. These model melts were accumulated over a pressure interval from 16 kb to 3 kb using the program SPIMW [*Kinzler and Grove*, 1992; *Kinzler*, 1997]. [4] Similar model melts to [3] but produced using the depleted mantle composition of *McDonough and Sun* [1995]. [5] A primitive EPR NMORB composition from the compilation in the GERM database (http://earthref.org/GERM/). [6] Xenolith intergranular melt. [7] Average of the range of recalculated olivine melt inclusions in the xenolith. The data for this figure are in Tables S9 and S10, where melt density and viscosity were calculated using the models of *Lange and Carmichael* [1987] and *Bottinga and Weill* [1972], respectively.

al., 1979; *McDonough and Sun*, 1995] with Ca/Na ratios that are higher than those observed in NMORB. For a given source composition, the Ca/Na ratios of the accumulated melt is a sensitive function of the increment of fractional melting. Using the program SPIMW [*Kinzler and Grove*, 1992; *Kinzler*, 1997] model melts produced by polybaric melting of depleted mantle peridotite (Table S9) under conditions that involve greater than 1% melt increments, and over a limited pressure range (16 kb to 3 kb), may have Ca/Na ratios greater than 11.5. However, these melts do not crystallize anorthite or calcic bytownite. Fractional crystallization modeling, using the program PETROLOG [*Danyushevsky*, 2001], shows that at crust-mantle depths these melts initially crystallize olivine followed by clinopyroxene prior to the appearance of plagioclase. Fractionation of clinopyroxene lowers the melt Ca/Na ratio so that the initial plagioclase to crystallize is either calcic labradorite or sodic bytownite. These models suggest that accumulated polybaric melts formed by >1% but <2% increments, i.e., <25% total source do not crystallize anorthite because of the early crystallization of clinopyroxene. In contrast, melts formed by 2% or greater incremental melting crystallize anorthite despite the early crystallization of clinopyroxene.

[29] Table S10 shows the liquid line of descent and crystallization products for a polybaric melt accumulation involving 2% incremental melting of a depleted mantle column between 16 kb and 3 kb pressure that undergoes fractional crystallization at the crust-mantle boundary (~3 kb pressure). The liquid line of descent with regard to plagioclase composition is also shown in Figure 16. In this particular case, the crystallization of olivine and clinopyroxene is followed by crystallization of anorthite and then bytownite. In the xenolith the anorthite composition is slightly less calcic than that shown by the model and zones outward to An_{86}, the most sodic composition observed at the Stage 1 resorption surface. The model suggests that the Stage 1 plagioclase crystallized over a temperature interval of ~25°C and the melt volume reduced by greater than 50%. During this interval both olivine and clinopyroxene must have been efficiently removed from the melt to produce a cumulate that was essentially pure plagioclase and intergranular liquid. This model is also consistent with calculations of melt composition and temperature using the parameterized equations of *Bédard* [2006]. For a dry melt, plagioclase of An_{95} composition (Table S10) crystallizes from a melt with MgO = 11.9 ± 2.0 wt.% at a temperature of 1250 ± 30°C. Plagioclase of An86 composition crystallizes from a melt with MgO = 9.86 ± 1.9 wt.% at a temperature of 1220 ± 21°C.

[30] The overwhelming volume of melt entering and maintaining the EPR magma system must be primitive NMORB in composition, based on observed MOR lava chemistry (Figure 15). However, we consider that the presence of anorthite-bytownite cumulates requires the addition of primitive melts with high Ca/Na ratios that are not initially part of the NMORB liquid line of descent. The anorthite xenocrysts observed in NMORB lavas are likely to be single crystals of disrupted anorthite cumulates within the MOR magma system. Such xenocrysts are relatively common in NMORB lavas [*Sinton et al.*, 1993; *Nielsen et al.*, 1995], suggesting that anorthite-bearing cumulates, and by inference calcic melts, may be a widespread component of EPR magma systems. No evidence for these primitive calcic melts exists in the lavas erupted at the NEPR, probably because they are volumetrically small relative to primitive NMORB. The liquid line of descent from primitive calcic melts, involving olivine and plagioclase precipitation, approaches, but is not identical to, the general liquid line of decent for NMORB. Thus mixing of small volumes of evolved calcic melt into a slightly evolved NMORB melt would effectively eliminate the former, but only slightly perturb the composition of the latter.

3.1.2. Stage 1 Plagioclase Dissolution

[31] Crenulated dissolution surfaces have only been observed within the bytownite zones of the Stage 1 cumulate plagioclase suggesting insufficient thermal energy to remelt anorthite. The resorption may have resulted from reheating of intergranular melt and the cumulus crystals by input of thermal energy from an external source, e.g., intrusion of hot basaltic melt in the proximity of the cumulate. Alternately, dissolution may have resulted from replacement of intergranular melt by hotter more primitive melt that may also have been undersaturated with regard to bytownite. Whatever the mechanism may have been, the result was a melt dominated plagioclase cumulate largely composed of anorthite.

3.2. Stage 2 Plagioclase

[32] Although the Stage 2 plagioclase contains patches of anorthite there is no clear textural evidence that this was a part of the original crystallization sequence, in contrast to the Stage 1 plagioclase crystallization. In fact, whatever compositional variability may have existed during the Stage 2 plagioclase crystallization has been overprinted. The Stage 2 plagioclases are dominantly bytownite in composition and extend to more sodic compositions than those observed in Stage 1. Two possibilities exist for this crystallization period. In the event that the dissolution of Stage 1 bytownite was due to reheating of intergranular melt then subsequent cooling of intergranular melt may have initiated a further period of bytownite crystallization. In other words, both Stage 1 and Stage 2 plagioclase were precipitated from the same melt but separated by a period of melt reheating. In the event that the intergranular melt was eviscerated then Stage 2 plagioclase precipitated from the replacement melt. In this case, precipitation of Stage 2 plagioclase from primitive, plagioclase-saturated NMORB remains a possibility.

3.2.1. Stage 2 Plagioclase Melting Reactions

3.2.1.1. Patchy Zoning

[33] The patchy zoning texture, and the sharp compositional contrasts between individual patches (Figure 8) are consistent with postsolidification

partial melting of Stage 2 plagioclase. All of these features are identical to those produced in plagioclase-melting experiments [*Johannes et al.*, 1994, Figure 2]. These authors interpret the development of patchy zoning within individual plagioclase crystals as the result of focused melting at crystal dislocation sites and describe the partial melting process as a solution/reprecipitation mechanism. This process results in a plagioclase melt phase more sodic and a reprecipitated solid phase more calcic than the original material. In the case of the Stage 2 plagioclase the reprecipitated solid phase accounts for the patches of anorthite. The patches of sodic bytownite represent melted plagioclase that subsequently partially solidified and the more calcic bytownite represents patches of the original unmelted plagioclase. This scenario suggests that after the precipitation of Stage 2 bytownite the cumulate underwent a period of reheating that caused partial melting of the Stage 2 plagioclase. Subsequent cooling caused the melted plagioclase to partially resolidify and preserved the patchy zoning texture.

3.2.1.2. Melt Inclusions in Stage 2 Plagioclase

[34] Although the melt inclusions in Stage 2 plagioclase have morphologies identical to those produced during plagioclase partial melting experiments [*Johannes et al.*, 1994] they do not have plagioclase compositions. Although they do not have basaltic compositions, their overall chemistry suggests the involvement of a basaltic melt in their formation. Most likely, an intergranular melt penetrated the partially melted Stage 2 plagioclase and the inclusions represent mixing of this melt with sodic plagioclase melt and subsequent partial reprecipitation of plagioclase. This latter process is suggested by the rims of bytownite that are commonly, but not invariably, observed around the melt inclusions suggesting that plagioclase precipitated on the walls of some inclusions.

[35] It is unlikely that the present intergranular melt or the melts represented by inclusions in olivine were involved in the formation of the plagioclase melt inclusions. The intergranular melt and olivine inclusion compositions lie close to the most aluminous end of the plagioclase inclusion population trend (Figure 13) and mixing with plagioclase melt would extend the inclusion composition trend toward high Al_2O_3 and CaO values, which is not observed. If the linear array of inclusion compositions is due to a mixing/precipitation mechanism then one might expect that some inclusion compositions would preserve the effects of mixing while others would show the effects of plagioclase precipitation. Thus the intergranular melt phase may have had a composition that was more primitive than either the olivine melt inclusions or the present intergranular melt, with both higher MgO, FeO (Figure 13) and lower CaO and Al_2O_3, i.e., a composition that lay further along the linear array of plagioclase inclusions. The more variable Na_2O would then reflect variable degrees of mixing of intergranular melt with sodic plagioclase partial melts having variable Na_2O contents.

3.2.2. Intergranular Melt

[36] The intergranular glass is marginally more evolved than the host glass, raising the possibility that the intergranular glass represents host glass that has infiltrated and partly disaggregated the xenolith. Although this is difficult to assess, there are chemical differences between them. First, the intergranular melt is enriched in TiO_2 and Na_2O relative to the host melt, which is consistent with the lower Mg#. Second, the intergranular melt was saturated with sulfide and precipitated droplets of sulfide. In contrast, the host melt was undersaturated with sulfide, shows a reaction relationship with xenolith sulfide and does not contain sulfide droplets within the glassy parts of the flow. In addition, the host glass surrounding the xenolith is completely devoid of vesicles, suggesting that the host melt did not exsolve a gas phase during ascent or upon eruption. The intergranular glass contains many vesicles, suggesting it readily exsolved a gas phase, probably CO_2, during ascent. It appears that the xenolith contained intergranular melt prior to being incorporated in the 1991 melt and has not simply been invaded by the host melt during transport.

3.3. Crystallization of Intergranular Olivine

[37] Fractional crystallization models, using PETROLOG, of melt inclusions in intergranular olivine indicate a melt liquidus temperature of ~1240°C and a period of olivine crystallization prior to the first appearance of plagioclase at ~1210°C. The observed variability of intergranular olivine compositions (~0.3 mol percent Fo) implies a temperature drop of ~10°C so the precipitation of olivine could not have been accompanied by the coprecipitation of plagioclase. Consequently, it is unlikely that the melt (or melts, see below) that crystallized olivine also precipitated the Stage 2 plagioclase. Textural relations between Stage 2 plagioclase and olivine are ambiguous. For instance, Stage 2 plagioclase does not enclose olivine suggesting that

the latter crystallized after the cessation of Stage 2 plagioclase crystallization. However, olivine may partly enclose plagioclase, and in some cases it appears that olivine has shielded Stage 1 plagioclase from growth of Stage 2 plagioclase (see Figure 3, lower center), suggesting that olivine may have crystallized prior to the precipitation of Stage 2 plagioclase. Recognizing these occasional textural ambiguities, the overall textural relations suggest that olivine precipitated in intergranular melt after the precipitation of Stage 2 plagioclase and occluded part of the pore structure. However, the olivine is too forsteritic to be in equilibrium with the present intergranular glass, although the latter is saturated with respect to olivine crystallization. This suggests that the intergranular melt must have been very close to its liquidus temperature during the period of time it was in contact with olivine, i.e., the melt had not cooled sufficiently to precipitate more olivine onto the rims of the interganular grains. This would also be consistent with the observation that the intergranular melt quenched to a crystal-free glass.

[38] The embayed outlines of all olivine grains may be due to either growth within limited volumes of melt or resorption. If the latter is the case then the cause, for instance reheating of interstitial melt as discussed above, may also have produced the partial remelting observed in Stage 2 plagioclase.

3.4. Melt Inclusions in Olivine

[39] The array of NEPR NMORB lavas erupted between 9°N and 10°N shown in Figure 12 principally reflects sequential fractional crystallization; initial crystallization of olivine from primitive NMORB followed by olivine and plagioclase, and then by olivine, plagioclase and clinopyroxene. On most binary oxide plots the melt inclusion populations do not lie within the field of NEPR MORB lavas, consequently they cannot be a part of the normal primitive NMORB liquid line of descent. They represent a more primitive, TiO_2-rich series of melts. Could these melts reflect assimilation of dunite or werhlite by NMORB that had evolved to more TiO_2-rich compositions? This would account for some of the chemical characteristics of the inclusions, e.g., high MgO and TiO_2, but would be at odds with the observation that the inclusion population lies within the Na_2O-TiO_2 array of NMORB. Possibly, selective assimilation of a small amount of ilmenite and/or titanomagnetite by a primitive NMORB melt (Mg# ~0.66) during percolation through an evolved crystal matrix could produce the melt inclusion population.

[40] The Type 1 and Type 2 inclusions crystallize between 4% and 6% olivine at 2–3 kb pressure prior to the appearance of clinopyroxene and then plagioclase so that a fractional crystallization relationship between the types could only involve olivine, but this scheme is inconsistent with their identical Mg# values. It appears that these melt inclusions record the passage of three distinct melt compositions that are not genetically related to each other, or to common NMORB melts, through any simple fractionation scheme.

3.5. Minor Phases

3.5.1. Spinel

[41] Cr spinel can be a sensitive indicator of petrogenesis [*Irvine*, 1967; *Arai*, 1992; *Clynne and Borg*, 1997] if primary crystal chemistry is preserved. Spinels commonly crystallize as the liquidus phase from basaltic melts, but their crystallization interval is short relative to the major silicate phases. Spinels undergo postcrystallization reactions as the melt cools [*Ridley*, 1977] unless shielded by other phases, normally olivine. (Mg, Fe)Al_2O_4 is replaced by Fe_2TiO_4 and Fe_3O_4 leading to an increase in Fe2O3 and consequently an increase in the Mg# value. The intergranular spinel, which appears to be the liquidus phase, is surrounded by glass so it is likely that quenching of the interstitial melt has largely preserved the original spinel composition. This is also consistent with the Mg#(spinel)/Mg#(melt) ratio being ~1.08, within the range of values observed in other basaltic glasses, and Fe^{2+}/Fe^{3+} ratios > 1.5 [*Clynne and Borg*, 1997].

[42] The presence of spinel inclusions in plagioclase is unusual because normally spinel crystallization ceases prior to the precipitation of plagioclase. The spinels observed as Stage 1 plagioclase inclusions are chemically different from the intergranular spinels in that they have substantially more Fe_2O_3 and higher Mg# values. These characteristics suggest that they have undergone a period of postcrystallization modification before being enveloped by the Stage 1 plagioclase.

3.5.2. Sulfide

[43] The crenulated margins of the larger droplets and lack of sulfide within the host glass are expected if the host melt was undersaturated with respect to sulfide precipitation. The absence of an

intermediate solid solution and hematite in the spongy contact zones with the host glass also suggests that the host melt was undersaturated with respect to sulfide precipitation and these phases were being resorbed into the host melt. This contrasts with the sulfide-saturated condition of the intergranular glass as indicated by the common presence of small sulfide blebs. This is consistent with the intergranular melt being slightly more chemically evolved than the host melt. Although attachment of the large sulfide droplets to the outer edge of the xenolith makes their genetic association with the xenolith equivocal, the observations above suggest that the large sulfide droplets are more likely a part of the xenolith assemblage rather than associated with the host melt. In a melt-dominated magma system large sulfide droplets would be expected to rapidly separate from the silicate phases. In the xenolith the large droplets may reflect the coagulation of small blebs and subsequent trapping in a crystal-dominated network of plagioclase crystals.

3.6. Preservation of the Xenolith

[44] Probably the most surprising aspect of the xenolith is that it has been preserved, along with many other similar xenoliths, during ascent through the magma system. An important reason may be that the xenolith appears to be especially "gassy" in that it contains several large vesicles. This may have provided the necessary buoyancy to prevent the xenolith from settling out of the host melt prior to eruption.

4. Broader Implications for Ocean Crust Forming Processes

[45] Lavas erupted at the ridge crest provide indirect and limited information on the magmatic processes that are currently building the oceanic crust beneath the ridge axis. Likewise, fragments of crust exposed off-axis provide information on the solid end-products of crustal formation but not on the complexities that result from melt-crystal interactions beneath the ridge axis. The xenolith captured by the 1991 lava flow is interpreted as a fragment of a melt-bearing plagioclase cumulate that forms a part of the nascent crust beneath the EPR. It is a member of a suite of melt-bearing anorthositic and troctolitic xenoliths captured in primitive NMORB lavas in the environs of 9°50′N on the NEPR. The xenolith is part of a crystal supported cumulate system and shows evidence, both directly and indirectly, for the passage of multiple melts of primitive NMORB composition through the network of intergranular pores. Two stages of plagioclase growth are recognized each followed by remelting and dissolution. Intergranular olivine may also have been resorbed. All of these features provide direct evidence of syntexis, a process previously inferred from the study of ophiolites [*Bédard*, 1993; *Bédard and Hébert*, 1996; *Bédard et al.*, 2000].

[46] The interpretation of anorthite crystallization from melts with high Ca/Na ratios implies that there are at least two different primitive melt types that enter the ridge magma system from the mantle. The dominant volumetric type is primitive NMORB that is the precursor of the common NMORB magmas erupted onto the seafloor. Evidence for the existence of primitive melts with high Ca/Na ratios that are not directly related to NMORB is cryptic, preserved only in the chemistry of highly calcic plagioclase. This evidence is not only preserved in the xenolith described here, but in anorthite xenocrysts in erupted NMORB and in anorthite cumulates in ophiolites.

[47] Overall, our results support the concept of the current AMC beneath the 9°50′N segment of the EPR as being composed of zones of crystal-magma mush. However, the xenolith texture and phase chemical data could be produced in either a sill or in a more diffuse zone of melt within a generally homogeneous zone of crystal mush. The large scale distribution of melt and crystals is, at this point, impossible to determine but the amount of liquid in this xenolith supports seismic and compliance measurements that indicate there is less than 18% melt on average in the lower crustal melt zone [*Crawford and Webb*, 2002]. However, seismic models suggest that melt proportions increase toward the top of the AMC where the mostly liquid magma lens resides. Clearly the mafic host magma acquired its chemical characteristics before entraining the xenolith in the lower crustal melt zone rather than evolving in the upper melt lens.

[48] Many "normal" lavas from the northern EPR (including the 9°30′–50′N section) contain multiple populations of plagioclase, olivine and, more rarely, clinopyroxene as well as crystal clots that have been interpreted as fragments of crystal networks formed in the mush zone of an AMC [*Pan and Batiza*, 2003]. Pan and Batiza conclude that the diverse chemical compositions of the crystals require mixing of distinct melts during their passage through a thick lower crustal mush zone and that the formation of most of the gabbroic layer is

unrelated to the shallow melt lens that caps the AMC. Evidence from some high-level gabbros from Oman suggests that primitive magmas can migrate to the axial melt lens with little or no differentiation and that the accretion of the lower crust primarily forms by subsidence after crystallization in the uppermost part of the AMC [*Coogan et al.*, 2002a]. *Natland and Dick* [2002] suggest the coarse anorthitic plagioclase phenocrysts that exist in some Indian Ocean lavas (but not in gabbros from Hole 735B) reflect early stages of crystallization and mixing of primitive magmas not recorded in the gabbros. They suggest that at slow-spreading centers there is little evidence for sill formation in the lower crust and that differentiation occurs during deformation of small nested plutons.

[49] Data presented here are consistent with the *Pan and Batiza* [2003] model and strongly support complex crystal-melt interactions between various melts and accumulating crystals in the lower crust and upper mantle. Such interactions have also been proposed based on mineralogic evidence in gabbroic sections formed at fast spreading centers (e.g., Hess Deep [*Natland and Dick*, 1996]) and from some ophiolites, e.g., Oman [*Kelemen et al.*, 1997]. These reactions cause changes in the composition of ascending melts and metasomatize the nascent oceanic crust (i.e., syntexis of *Bédard and Hébert* [1996] and *Bédard et al.* [2000]). Our results provide more constraints to the ongoing debate regarding the development of the plutonic foundations of the oceanic crust and the mechanisms of magmatic differentiation that occur within oceanic crust. Given the reactive processes that we propose are common beneath the EPR it is perhaps surprising that they are not reflected (or that we do not recognize them) in the erupted lavas. There is ample evidence from trace element and isotopic data from EPR glasses that mixing of primitive and more evolved magmas occurs as well as mixing between enriched and depleted magmas, but the geochemical effects of the reactive porous flow that we describe here have yet to be defined in terms of lava chemistry.

[50] Perhaps the most important characteristic of the xenolith is the abundance of cumulate anorthite, which implies a sufficient volume of calcic melt to promote accumulation of plagioclase crystals. Thus the xenolith confirms the presence of calcic melts within the axial magma system, based upon melt inclusions in highly calcic plagioclase xenocrysts [*Sinton et al.*, 1993; *Nielsen et al.*, 1995]. We suggest that primitive melts with high Ca/Na ratios are commonly formed in the subridge depleted mantle as part of the polybaric, fractional melting process, but are less voluminous than typical primitive NMORB. Despite the growing evidence for the presence of melts sufficiently calcic to precipitate anorthite, magmas of this type are not observed in lavas erupted at MORs and sampled to date. The crystalline products are preserved but not the associated melts. An explanation may lie in the buffering effect of the crystalline mush zones during melt transport through the nascent crust. Mixing with the more voluminous NMORB melts may also effectively remove the calcic melts but effect the NMORB compositions to a minor degree. The process of remelting of plagioclase cumulates and mixing with interstitial melt has been caught in the act within the xenolith confirming that this process can explain the cryptic plagioclase signatures observed in some melt inclusions [*Danyushevsky et al.*, 2003]. Another potential consequence of syntactic reactions involving plagioclase relates to the chemistry of primitive high-MgO glasses that are observed in leaky transforms that off-set the NEPR and seamount lavas [*Allan et al.*, 1989; *Perfit et al.*, 1996]. These are anomalously aluminous compared to NMORB and are spatially associated with enriched lavas that are unlike MORB. In the 9°–10°N area, it appears that both more and less incompatible element enriched lavas are erupted off-axis because they avoid extensive mixing in the high level axial magma reservoir. Consequently, the depleted magmas maintain chemical characteristics that reflect both mantle and crustal processes. The primitive high-MgO melts are strongly undersaturated with respect to plagioclase and their aluminous nature may reflect resorption of plagioclase as they percolate through the axial magma system.

[51] Diffusive interaction of percolating melt with gabbroic cumulates (plagioclase + olivine + clinopyroxene) has been modeled to producing the measured ^{226}Ra-^{230}Th disequilibrium in young oceanic volcanics [*Saal and Van Orman*, 2004; *Van Orman et al.*, 2006]. Of particular importance are melt interactions with plagioclase because this mineral hosts most of the ^{226}Ra [*Van Orman et al.*, 2006]. For melts that are in equilibrium with the cumulate minerals, isotopic exchange with melt phase involves solid state diffusion through the various cumulate minerals. However, ^{226}Ra-^{230}Th disequilibrium is likely to be modified if the melt phase is not in equilibrium with the solid matrix. Here, we have shown that melts percolating

through a cumulate plagioclase matrix cause resorption of plagioclase into the melt phase so the isotopic characteristics of the plagioclase would be transferred quantitatively into the melt without involving diffusion. This might have a substantial influence on U-series disequilibrium in the melt if the plagioclase to melt volume ratio was large. In addition, the xenolith shows evidence for melting and recrystallization of solid plagioclase crystals, presumably as an intermediate step in the resorption process. Consequently, the redistribution of U-series isotopes would be substantially faster as it would involve melt-melt rather than melt-solid diffusion.

5. Summary

[52] A xenolith collected from the 1991 flow on the NEPR at 9°50′N records the evolution of an olivine anorthosite. It is a fragment of a cumulate lithology that currently exists in the magma system beneath the neovolcanic zone of the NEPR at this locality. A complex petrologic history is indicated, as follows. The cumulate includes two generations of plagioclase growth. The first stage (Stage 1) involved accumulation of anorthite-bytownite crystals that may have formed a matrix-dominated cumulate pile. This was followed by a period of plagioclase resorption that resulted in a melt-dominated system. The second stage (Stage 2) of plagioclase growth may have occurred in situ and principally involved growth of bytownite onto the remaining crystals of the first stage. The Stage 1 plagioclase growth, and probably also the Stage 2 also, record the presence of a primitive calcic melt that was not directly related to primitive NMORB. At the culmination of plagioclase crystallization the cumulate was again matrix-dominated and contained at least 20% intergranular porosity. The intergranular porosity was partly occluded by the growth of olivine from at least three different intergranular melts of primitive composition that generally have NMORB-like compositions. None of these melts have compositions within the NMORB liquid line of descent observed in lavas from this part of the NEPR. During the ascent of hot melts through the pore structure the Stage 2 plagioclase was partially remelted and a patchy zoning developed that obliterated the original compositional zoning. The Stage 2 plagioclase was also infiltrated with intergranular melt preserved as melt inclusions that give the Stage 2 plagioclase a distinctive sieve texture. The pore volume was finally eviscerated by a moderately primitive NMORB melt now preserved as intergranular glass. The xenolith was captured in another moderately primitive melt and the intergranular glass exsolved a gas phase that may have increased its buoyancy and allowed the xenolith to be carried to the surface.

Acknowledgments

[53] Lawrence Coogan and Jean Bédard provided careful and insightful journal reviews that greatly improved the manuscript. We thank John Maclennan for helpful comments on a draft of the manuscript and Vincent Salters for editorial support. We thank the crew of the Atlantis II and pilots of Alvin for their expertise at sea. The Mineral Resources Program, USGS, provided support to W.I.R. for this research. Field and laboratory research was supported by NSF grants OCE-9402360, 9403773, and 0138088 to M.R.P. and NSF grants OCE-9819261 and OCE-0525863 to D.J.F. W.I.R. publishes with permission of the Director, U.S. Geological Survey.

References

Allan, J. F., R. Batiza, M. R. Perfit, D. J. Fornari, and R. O. Sack (1989), Petrology of lavas from the Lamont seamount chain and adjacent East pacific Rise, 10°N, *J. Petrol.*, *30*, 1245–1298.

Arai, S. (1992), Chemistry of spinels in volcanic rocks as a potential guide to magma chemistry, *Mineral. Mag.*, *56*, 174–184.

Batiza, R., and Y. Niu (1992), Petrology and magma chambers processes at the East Pacific Rise ~9 deg 30′N, *J. Geophys. Res.*, *87*, 6779–6797.

Bédard, J. H. (1993), Oceanic crust as a reactive filter: Synkinematic intrusion, hybridization, and assimilation in an ophiolitic magma chamber, western Newfoundland, *Geology*, *21*, 77–80.

Bédard, J. H. (2006), Trace element partitioning in plagioclase feldspar, *Geochim. Cosmochim. Acta*, *70*, 3717–3742.

Bédard, J. H., and R. Hébert (1996), The lower crust of the Bay of Islands ophiolite, Canada: Petrology, mineralogy, and the importance of syntexis in magmatic differentiation in ophiolites and at ocean ridges, *J. Geophys. Res.*, *101*, 25,105–25,124.

Bédard, J. H., R. Hebert, A. Berclaz, and V. Varfalvy (2000), Syntexis and the genesis of lower oceanic crust, *Spec. Pap. Geol. Soc. Am.*, *349*, 105–119.

Bender, J. F., D. M. Miller, and C. H. Langmuir (1991), Gabbroic xenoliths from 9°20′N–10°00′N on the East Pacific Rise suggests in situ crystallization, *Eos Trans. AGU*, *72*, 496.

Borisov, A. A., and A. I. Shapkin (1990), A new empirical equation rating Fe3+/Fe2+ in magmas to their composition, oxygen fugacity, and temperature, *Geochem. Int.*, *27*, 11–116.

Boudier, F., A. Nicolas, and B. Ildefonse (1996), Magma chambers in the Oman ophiolite: Fed from the top and the bottom, *Earth Planet Sci. Lett.*, *144*, 239–250.

Bottinga, Y., and D. F. Weill (1972), The viscosity of magmatic silicate liquids: A model for calculation, *Am. J. Sci.*, *272*, 438–475.

Clynne, M. A., and L. E. Borg (1997), Olivine and chromium spinel in primitive calc-alkaline and tholeiitic lavas from the southernmost Cascade Range, California: A reflection of relative fertility of the source, *Can. Mineral.*, *35*, 453–472.

Coogan, L. A., A. D. Saunders, P. D. Kempton, and M. J. Norry (2000), Evidence from oceanic gabbros for porous melt migration within a crystal mush beneath the Mid-Atlantic Ridge, *Geochem. Geophys. Geosyst.*, *1*(9), doi:10.1029/2000GC000072.

Coogan, L. A., G. Thompson, and C. J. Macleod (2002a), A textural and geochemical investigation of high level gabbros from the Oman ophiolite: Implications for the role of the axial magma chamber at fast-spreading ridges, *Lithos*, *63*, 67–82.

Coogan, L. A., K. M. Gillis, C. J. MacLeod, G. M. Thompson, and R. Hékinian (2002b), Petrology and geochemistry of the lower ocean crust formed at the East Pacific Rise and exposed at Hess Deep: A synthesis and new results, *Geochem. Geophys. Geosyst.*, *3*(11), 8604, doi:10.1029/2001GC000230.

Coogan, L. A., G. J. Banks, K. M. Gillis, C. J. Macleod, and J. A. Pearce (2003a), Hidden melt signatures recorded in the Troodos ophiolite plutonic suite: Evidence for widespread generation of depleted melts and intra-crustal melt signatures, *Contrib. Mineral. Petrol.*, *144*, 484–505.

Coogan, L. A., G. Thompson, and C. J. MacLeod (2003b), A textural and geochemical investigation of high level gabbros from the Oman ophiolite: Implication for the role of the axial magma chamber at fast spreading ridges, *Lithos*, *63*, 67–82.

Costa, F., S. Chakrabouty, and R. Dohman (2003), Diffusion coupling between trace and major elements and a model for calculation of magma residence times using plagioclase, *Geochim. Cosmochim. Acta*, *67*, 2189–2200.

Crawford, W. C., and S. C. Webb (2002), Variations in the distribution of magma in the lower crust and at the Moho beneath the East Pacific Rise at 9°–10°N, *Earth Planet. Sci. Lett.*, *203*, 117–130.

Crawford, W. C., S. C. Webb, and J. A. Hildebrand (1999), Constraints on melt in the lower crust and Moho at the East Pacific Rise, 9°48′N, using seafloor compliance measurements, *J. Geophys. Res.*, *104*, 2923–2939.

Danyushevsky, L. V. (2001), The effects of small amounts of H_2O on crystallization of mid-ocean ridge and backarc basin magmas, *J. Volcanol. Geotherm. Res.*, *110*, 265–280.

Danyushevsky, L. V., A. V. Sobolev, and L. V. Dmitriev (1996), Estimation of the pressure of crystallization and H_2O content of MORB and BABB glasses: Calibration of an empirical technique, *Mineral. Petrol.*, *57*, 185–204.

Danyushevsky, L. V., M. R. Perfit, S. M. Eggins, and T. J. Falloon (2003), Crustal origin for coupled "ultradepleted" and "plagioclase" signatures in MORB olivine-hosted melt inclusions: Evidence from the Siqueiros Transform Fault, East Pacific Rise, *Contrib. Mineral. Petrol.*, *144*, 619–637.

Davis, A. S., and D. A. Clague (1990), Gabbroic xenoliths from the northern Gorda Ridge: Implications for magma chamber processes under slow spreading centers, *J. Geophys. Res.*, *95*, 10,885–10,905.

Detrick, R. S., P. Buhl, E. Vera, J. Mutter, J. Orcutt, J. Madsen, and T. Brocher (1987), Multi-channel seismic imaging of a crustal magma chamber along the East Pacific Rise, *Nature*, *326*, 35–41.

Detrick, R. S., G. M. Purdy, S. C. Solomon, and S. D. Wilcock (1990), The three-dimensional seismic velocity structure of the East Pacific Rise near latitude 9°30′N, *Nature*, *347*, 639–645.

Dick, H. J. B., et al. (2002), Primary silicate mineral chemistry of a 1.5-km section of very slow spreading lower ocean crust: ODP Hole 735B, Southwest Indian Ridge, in *Proceedings of the Ocean Drilling Program, Scientific Results* [online], vol. 176, edited by J. H. Natland et al., 61 pp. (Available at http://www-odp.tamu.edu/publications/176_SR/VOLUME/CHAPTERS/SR176_10.PDF)

Dixon, J. E., D. A. Clague, and J.-P. Eissen (1986), Gabbroic xenoliths and host ferrobasalt from the Southern Juan de Fuca Ridge, *J. Geophys. Res.*, *91*, 3795–3820.

Dunn, R. A., and D. R. Toomey (2000), Three-dimensional seismic structure and physical properties of the crust and shallow mantle beneath the East Pacific Rise at 9°30′N, *J. Geophys. Res.*, *105*(B10), 23,537–23,555.

Elthon, D. (1979), High magnesia liquids as the parental magma for ocean floor basalts, *Nature*, *278*, 514–518.

Elthon, D., and C. M. Scarfe (1984), High-pressure phase equilibria of a high-magnesia basalt and the genesis of primary oceanic basalts, *Am. Mineral.*, *69*, 1–15.

Falloon, T. J., D. H. Green, A. L. Jacques, and J. W. Hawkins (1998), Refractory magmas in back-arc basin settings-experimental constraints on the petrogenesis of a Lau Basin example, *J. Petrol.*, *40*, 255–277.

Ford, C. E., D. G. Russel, J. A. Groven, and M. R. Fisk (1983), Distribution coefficients of Mg^{2+}, Fe^{2+}, Ca^{2+} and Mn^{2+} between olivine and melt, *J. Petrol.*, *24*, 256–265.

Fornari, D. J., R. M. Haymon, M. R. Perfit, T. K. P. Gregg, and M. H. Edwards (1998), Axial summit trough of the East Pacific Rise 9°–10°N: Geological characteristics and evolution of the axial zone on fast-spreading mid-ocean ridges, *J. Geophys. Res.*, *103*, 9827–9855.

Garmany, J. (1989), Accumulation of melt at the base of young oceanic crust, *Nature*, *340*, 628–632.

Gregg, T. K. P., D. J. Fornari, M. R. Perfit, R. M. Haymon, and J. H. Fink (1993), Rapid emplacement of a mid-ocean ridge lava flow on the East Pacific Rise at 9°46′–51′N, *Earth Planet. Sci. Lett.*, *144*, 1–7.

Grove, T. L., R. J. Kinzler, and W. B. Bryan (1992), Fractionation of mid-ocean ridge basalts, in *Mantle Flow and Melt Generation at Mid-Ocean Ridges*, *Geophys. Monogr. Ser.*, vol. 71, edited by J. Phipps Morgan, D. K. Blackman, and J. Sinton, pp. 281–310, AGU, Washington, D. C.

Gurenko, A. A., and A. V. Sobolev (2006), Crust-primitive magma interaction beneath neovolcanic rift zone of Iceland recorded in gabbro xenoliths from Midfell, SW Iceland, *Contrib. Mineral. Petrol.*, *151*, 495–520.

Hekinian, R., R. Hebert, R. C. Maury, and E. T. Berger (1986), Othopyroxene-bearing gabbroic xenoliths in basalts from the East Pacific Rise axis near 12°50′N, *Bull. Mineral.*, *108*, 691–698.

Hussenoeder, S. A., J. A. Collins, G. M. Kent, R. S. Detrick, A. J. Harding, J. A. Orcutt, J. C. Mutter, and P. Buhl (1996), Seismic analysis of the axial magma chamber reflector along the southern East Pacific Rise from conventional reflection profiling, *J. Geophys. Res.*, *101*, 22,087–22,105.

Irvine, T. N. (1967), Chromium spinel as a petrogenetic indicator, Part 2: Petrologic applications, *Can. J. Earth Sci.*, *4*, 71–103.

Jagoutz, E., H. Palme, H. Baddenhausen, K. Blum, M. Cendales, G. Dreibus, B. Spettel, V. Lorenz, and H. Wanke (1979), The abundances of major, minor, and trace elements in the Earth's mantle as derived from primitive ultramafic nodules, in *Proceedings of the 10th Lunar and Planetary Science Conference*, *Geochim. Cosmochim. Acta*, *11*, suppl., 2031–2050.

Johannes, W., J. Koepke, and H. Behrens (1994), Partial melting reactions of plagioclase and plagioclase-bearing systems, in *Feldspars and Their Reactions*, edited by I. Parson, pp. 161–194, Springer, New York.

Karson, J. A., et al. (2002), Structure of uppermost fast-spread oceanic crust exposed at the Hess Deep Rift: Implications for subaxial processes at the East Pacific Rise, *Geochem. Geophys. Geosyst.*, *3*(1), 1002, doi:10.1029/2001GC000155.

Kelemen, P. B., K. Koga, and N. Shimuzu (1997), Geochemistry of gabbro sills in the crust/mantle transition zone of the Oman ophiolite: Implications for the origin of the oceanic crust, *Earth Planet. Sci. Lett.*, *146*, 475–488.

Kent, G. M., A. J. Harding, and J. A. Orcutt (1990), Evidence for a smaller magma chamber beneath the East Pacific Rise at 9°30′ N, *Nature*, *344*, 650–653.

Kent, G. M., A. J. Harding, and J. A. Orcutt (1993), Distribution of magma beneath the East Pacific Rise between the Clipperton transform and the 9°17′N deval from forward modeling of common depth point data, *J. Geophys. Res.*, *98*, 13,945–13,969.

Kinzler, R. J. (1997), Melting of mantle peridotite at pressures approaching the spinel to garnet transition: Application to mid-ocean ridge basalt petrogenesis, *J. Geophys. Res.*, *102*, 853–874.

Kinzler, K. J., and T. L. Grove (1992), Primary magmas of mid-ocean ridge basalts: 2. Applications, *J. Geophys. Res.*, *97*, 6907–6926.

Koga, K. T., P. B. Kelemen, and N. Shimizu (2001), Petrogenesis of the crust-mantle transition zone and the origin of lower crustal wehrlite in the Oman ophiolite, *Geochem. Geophys. Geosyst.*, *2*(9), doi:10.1029/2000GC000132.

Korenaga, J., and P. B. Kelemen (1997), Origin of gabbro sills in the Moho transition zone of the Oman ophiolite: Implications for magma transport in the oceanic lower crust, *J. Geophys. Res*, *102*, 27,729–27,749.

Korenaga, J., and P. B. Kelemen (1998), Melt migration through the oceanic lower crust: A constraint from melt percolation modeling with finite solid diffusion, *Earth Planet. Sci. Lett.*, *156*, 1–11.

Lange, R. A., and I. S. E. Carmichael (1987), Densities of Na_2O-K_2O-CaO-MgO-FeO-Fe_2O_3–Al_2O_3–TiO_2–SiO_2 liquids: New measurements and derived partial molar properties, *Geochim. Cosmochim. Acta*, *51*, 2931–2946.

Langmuir, C. H., J. F. Bender, and R. Batiza (1986), Petrological and tectonic segmentation of the East Pacific Rise, 5°30′–14°30′N, *Nature*, *322*, 422–429.

Le Maitre, R. W. (1989), *A Classification of Igneous Rocks and Glossary of Terms*, 193 pp., Blackwell Sci., Malden, Mass.

Lundstrom, C., A. Boudreau, and M. Pertermann (2005), Diffusion-reaction in a thermal gradient: Implications for the genesis of anorthitic plagioclase, high alumina basalt and igneous mineral layering, *Earth Planet Sci. Lett.*, *237*, 829–854.

Macleod, C. J., and G. Yaouancq (2000), A fossil melt lens in the Oman ophiolite: Implications for magma chamber processes at fast spreading ridges, *Earth Planet. Sci. Lett.*, *176*, 357–373.

Macleod, C. J., F. Boudier, G. Yaoancq, and C. Richter (1996), Gabbro fabrics from ODP Site 894, Hess Deep: Implications for magma chamber processes at the East Pacific Rise, *Proc. Ocean Drill. Program Sci. Results*, *147*, 317–328.

Marsh, B. D. (2000), Magma chambers, in *Encyclopedia of Volcanoes*, edited by H. Sigurdsson, pp. 191–206, Elsevier, New York.

Marsh, B. (2004), A magmatic mush column Rosetta Stone: The McMurdo Dry Valleys of Antarctica, *Eos Trans. AGU*, *85*(47), 497.

McDonough, W. F., and S.-S. Sun (1995), The composition of the Earth, *Chem. Geol.*, *120*, 223–253.

Miller, D. M. (1995), Appendix A: Gabbroic xenoliths from a crystallizing boundary layer beneath the East Pacific Rise, in Petrogenesis of adjacent calc-alkaline and tholeiitic volcanoes on Umnak Island in the Aleutian Arc, Alaska, Ph.D. thesis, pp. 366–417, Columbia Univ., New York.

Natland, J. H., and H. J. B. Dick (1996), Melt migration through high-level gabbroic cumulates of the East Pacific Rise at Hess Deep: The origin of magma lenses and the deep crustal structure of fast-spreading ridges, *Proc. Ocean Drill. Program Sci. Results*, *147*, 21–58.

Natland, J. H., and H. J. B. Dick (2002), Stratigraphy and composition of gabbros drilled in Ocean Drilling Program Hole 735B, Southwest Indian Ridge: A synthesis of geochemical data, in *Proceedings of the Ocean Drilling Program, Scientific Results* [online], vol. 176, edited by J. H. Natland et al., 69 pp. (Available at http://www-odp.tamu.edu/publications/176_SR/VOLUME/SYNTH/SYNTH.PDF)

Nicolas, A. (1989), *Structures of Ophiolites and Dynamics of Oceanic Lithosphere*, 367 pp., Springer, New York.

Nicolas, A., I. Reuber, and K. Benn (1987), A new magma chamber model based on structural studies in the Oman ophiolite, *Tectonophysics.*, *151*, 87–105.

Nielsen, R., J. Crum, R. Bourgeois, K. Hascall, L. M. Forsythe, M. R. Fisk, and D. M. Christie (1995), Melt inclusions in high-An plagioclase from the Gorda Ridge: An example of the local diversity of MORB parent magmas, *Contrib. Mineral. Petrol.*, *122*, 34–50.

Pan, Y., and R. Batiza (2003), Magmatic processes under mid-ocean ridges: A detailed mineralogic study of lavas from East Pacific Rise 9°30′N, 10°30′N, and 11°20′N, *Geochem. Geophys. Geosyst.*, *4*(11), 8623, doi:10.1029/2002GC000309.

Perfit, M. R., and W. W. Chadwick (1998), Magmatism at the mid-ocean ridges: Constraints from volcanological and geochemical investigations, in *Faulting and Magmatism at Mid-Ocean Ridges*, *Geophys. Monogr. Ser.*, vol. 106, edited by W. R. Buck et al., pp. 57–115, Washington, D. C.

Perfit, M. R., D. J. Fornari, M. C. Smith, J. F. Bender, C. H. Langmuir, and R. M. Haymon (1994), Small-scale spatial and temporal variations in mid-ocean ridge crest magmatic processes, *Geology*, *22*, 375–379.

Perfit, M. R., et al. (1996), Recent volcanism in the Siqueiros transform fault: Picritic basalts and implications for MORB magma genesis, *Earth Planet. Sci. Lett.*, *141*, 91–108.

Ridley, W. I. (1977), The crystallization trends of spinels in Tertiary basalts from Rhum and Muck and their petrogenetic significance, *Contrib. Mineral Petrol.*, *64*, 243–255.

Rubin, K. H., J. D. Macdougall, and M. R. Perfit (1994), ^{210}Po–^{210}Pb dating of recent volcanic eruptions on the seafloor, *Nature*, *369*, 841–844.

Saal, A. E., and J. A. Van Orman (2004), The ^{226}Ra enrichment in oceanic basalts: Evidence for melt-cumulate diffusive interaction processes within the oceanic lithosphere, *Geochem. Geophys. Geosyst.*, *5*, Q02008, doi:10.1029/2003GC000620.

Schouten, H., and P. B. Kelemen (2002), Melt viscosity, temperature and transport processes, Troodos ophiolite, Cyprus, *Earth Planet. Sci.*, *201*, 337–352.

Singh, S. C., G. M. Kent, J. S. Collier, A. J. Harding, and J. A. Orcutt (1998), Melt to mush variations in crustal magma

properties along the ridge crest at the southern East Pacific Rise, *Nature*, *394*, 874–878.

Sinton, C. W., D. M. Christie, V. L. Coombs, R. L. Nielsen, and M. R. Fisk (1993), Near-primary melt inclusions in anorthite phenocrysts from the Galapagos Platform, *Earth Planet. Sci. Lett.*, *119*, 527–537.

Sinton, J. M., and R. S. Detrick (1992), Mid-ocean ridge magma chambers, *J. Geophys. Res.*, *97*, 197–216.

Smith, M. C. (1993), Petrologic and geochemical; investigations of basalts from the southern Juan de Fuca Ridge, Ph.D. thesis, Univ. of Fla., Gainesville.

Smith, M. C., M. R. Perfit, and I. R. Jonasson (1994), Petrology and geochemistry of basalts from the southern Juan de Fuca Ridge: Controls on the spatial and temporal evolution of mid-ocean ridge basalt, *J. Geophys. Res.*, *99*, 4787–4812.

Smith, M. C., M. R. Perfit, D. J. Fornari, W. I. Ridley, M. H. Edwards, G. J. Kurras, and K. L. Von Damm (2001), Magmatic processes and segmentation at a fast spreading mid-ocean ridge: Detailed investigation of an axial discontinuity on the East Pacific Rise crest at 9°37′N, *Geochem. Geophys. Geosyst.*, *2*(10), doi:10.1029/2000GC000134.

Van Orman, J. A., A. E. Saal, B. Bourdon, and E. H. Hauri (2006), Diffusive fractionation of U-series radionuclides during mantle melting and shallow-level melt-cumulate interaction, *Geochim. Cosmochim. Acta*, *70*, 4797–4812.